DOI: 10.1002/cplu.201402006

Synthesis and Electron-Transfer Processes in a New Family of Ligands for Coupled Ru–Mn_2 Complexes

Erik A. Karlsson,[a] Bao-Lin Lee,[a] Rong-Zhen Liao,[a] Torbjörn Åkermark,[a] Markus D. Kärkäs,[a] Valeria Saavedra Becerril,[b] Per E. M. Siegbahn,[a] Xiaodong Zou,[c] Maria Abrahamsson,*[b] and Björn Åkermark*[a]

A series of $[Ru(bpy)_3]^{2+}$-type (bpy = 2,2′-bipyridine) photosensitisers have been coupled to a ligand for Mn, which is expected to give a dinuclear complex that is active as a water oxidation catalyst. Unexpectedly, photophysical studies showed that the assemblies had very short lived excited states and that the decay patterns were complex and strongly dependent on pH. One dyad was prepared that was capable of catalysing chemical water oxidation by using $[Ru(bpy)_3]^{3+}$ as an oxidant. However, photochemical water oxidation in the presence of an external electron acceptor failed, presumably because the short excited-state lifetime precluded initial electron transfer to the added acceptor. The photophysical behaviour could be explained by the presence of an intricate excited-state manifold, as also suggested by time-dependent DFT calculations.

Introduction

With growing awareness of the limitations and disadvantages of the energy sources that form the basis for today's society, interest in exploring alternative energy systems is increasing. One approach to develop systems for fuel production would be to mimic the charge-separation processes in photosystem II (PS II).[1–5] This multi-component protein complex uses light for the extraction of electrons from water to generate biomass from carbon dioxide. The oxygen evolving complex (OEC) is responsible for carrying out the oxidation of H_2O and consists of a tetranuclear manganese cluster.[6] Inspired by natural systems, several artificial water oxidation catalysts (WOCs) have been developed, based on a range of different metals.[7–29] In addition, a few model systems for photoinduced electron transfer from manganese complexes to a chromophore have been prepared and characterised.[30–45] Typically, metal porphyrins or $[Ru(bpy)_3]^{2+}$-type (bpy = 2,2′-bipyridine) photosensitisers have been used as chromophores (photosensitisers), which upon excitation can transfer an electron to an external acceptor. The photosensitiser is subsequently regenerated by electron transfer from a nearby electron donor, such as an attached manganese complex. We have previously prepared a series of ruthenium–manganese dyads, but none of them proved capable of catalysing the oxidation of water, which requires the consecutive transfer of four electrons.[46] This is most likely to be related to degradation of the ligands.

However, we have recently managed to prepare a dinuclear manganese complex (**1**), which does catalyse water oxidation (Figure 1).[47] We therefore decided to try to prepare ruthenium–manganese dyads; this involved coupling of this dinuclear Mn unit to a $[Ru(bpy)_3]^{2+}$-type photosensitiser. Herein, we present the synthesis, characterisation, and electrochemical and photophysical properties of the ligand complexes **7a**–**c**. The complexes **7a** and **7b** were first prepared, but turned out to have unexpected and unusual photochemistry, with very short excited-state lifetimes. It seemed likely that this was due to the large conjugated systems and complex **7c** was therefore prepared with the hope that the phenyl substituent on the central imidazole would decrease the planarity owing to steric strain. However, this complex also had a very short excited-state lifetime. These results were rather unexpected and prompted us to study the photophysical properties of the complexes in more detail, and also investigate the structural and electronic properties by means of time-dependent density functional theory (TDDFT) calculations.

We also prepared dyad **8**, although it seemed unlikely that this would have a longer lifetime. It seemed interesting, nonetheless, to see if this complex could catalyse water oxidation, either chemically or by light induction.

[a] Dr. E. A. Karlsson, Dr. B.-L. Lee, Dr. R.-Z. Liao, Dr. T. Åkermark, Dr. M. D. Kärkäs, Prof. P. E. M. Siegbahn, Prof. B. Åkermark
Department of Organic Chemistry
Arrhenius Laboratory, Stockholm University
106 91 Stockholm (Sweden)
E-mail: bjorn.akermark@organ.su.se

[b] V. S. Becerril, Prof. M. Abrahamsson
Department of Chemical and Biological Engineering
Chalmers University of Technology
412 96 Gothenburg (Sweden)
E-mail: abmaria@chalmers.se

[c] Prof. X. Zou
Department of Materials and Environmental Chemistry
Arrhenius Laboratory, Stockholm University
106 91 Stockholm (Sweden)

Supporting information for this article is available on the WWW under http://dx.doi.org/10.1002/cplu.201402006.

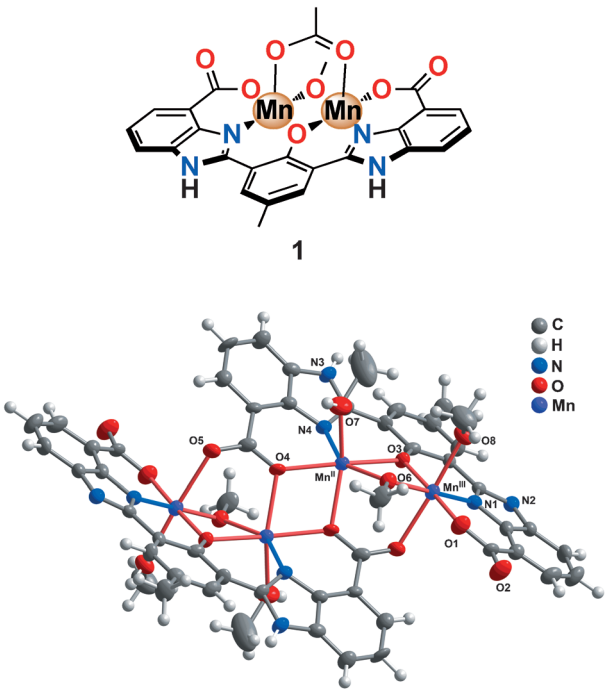

Figure 1. The previously reported dinuclear manganese-based WOC **1** (top) and the crystal structure of the tetranuclear manganese complex generated from complex **1** (bottom). Ellipsoids are displayed at the 50% probability level.

Results and Discussion

Synthesis

The preparation of ligand complexes **7a–c** and dyad **8** is depicted in Scheme 1. The synthesis is based on the reaction of 1,10-phenanthroline-5,6-dione (**2**) with *p*-hydroxybenzaldehyde and ammonium acetate to yield compound **3a**. In the presence of aniline, this reaction gave the N-arylated product **3b**. Reaction of **3a** with the ruthenium precursor in ethylene glycol at 120 °C gave complex **5a** as the triflate salt. To avoid transesterification, the reactions of precursor **4b** with compounds **3a** and **3b** were performed in ethanol at 120 °C to yield complexes **5b** and **5c**, respectively. Treatment of complexes **5a–c** with 20 molar equivalents of hexamethylenetetramine in TFA at 120 °C for 3 days, followed by hydrolysis of the intermediate imines by aqueous HCl, gave the diformylated ruthenium complexes **6a–c** as salts containing a mixture of triflate and trifluoroacetate counterions. Finally, a reductive cyclisation with 2-amino-3-nitrobenzoic acid in a solution of water/ethanol, with sodium dithionite as the reducing agent, gave the desired ruthenium complexes **7a–c**. The coupled Ru–Mn_2 dyad **8**, which was essentially insoluble in organic solvents, was then obtained by using a Soxhlet extractor to slowly extract the ligand complex **7c** into a solution of methanol containing $Mn(OAc)_2{\cdot}4H_2O$ and NaOAc.

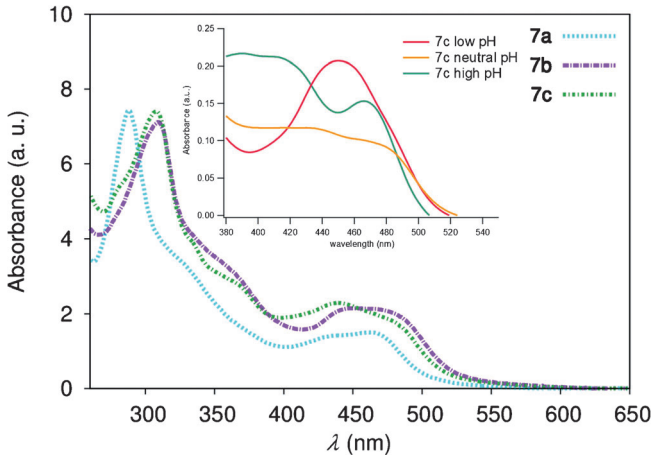

Figure 2. Absorption spectra of complexes **7a–c** in a 1:1 mixture of acetonitrile/water (v/v). The inset shows the metal-to-ligand charge-transfer (MLCT) region for **7c** at different pH values.

UV/Vis spectroscopy

The electronic absorption spectra of **7a–c** in a 1:1 mixture of acetonitrile/water (v/v) are shown in Figure 2. They all display an intense band at around $\lambda \approx 300$ nm, corresponding to the π–π^* transitions in the bpy ligands, as also demonstrated by ligands **3** and complexes **5** (Figure S1 in the Supporting Information). The introduction of the ruthenium moiety adds a broad MLCT band centred at $\lambda \approx 450$ nm, which partly overlaps with the imidazole absorption at $\lambda \approx 350$ nm (Figure 2 and Figure S1 in the Supporting Information). The results are consistent with published data[43,48] and our TDDFT calculations (see below). The MLCT band is sensitive to pH, as shown by the inset in Figure 2. The UV/Vis spectrum of dyad **8** is very similar to that of ligand **7c** (Figure 3), although **8** has a higher absorption at $\lambda \approx 400$ nm, for which the manganese imidazole complex has a distinct absorption (Figure S2 in the Supporting Information) and confirms the coordination of manganese in dyad **8**.

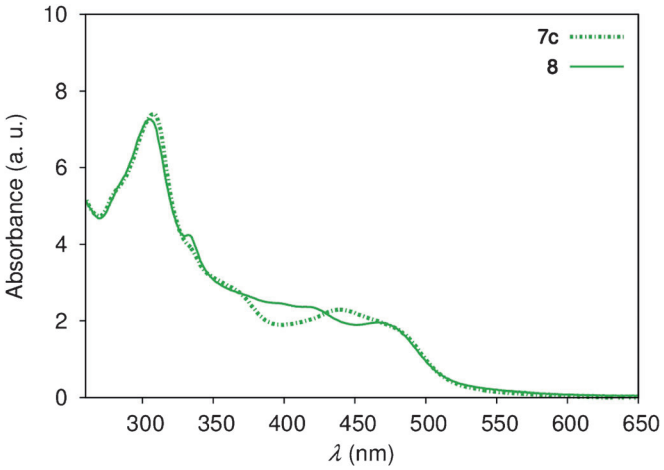

Figure 3. Comparison of the absorption spectra of complexes **7c** and **8c** in a 1:1 mixture of acetonitrile/water (v/v).

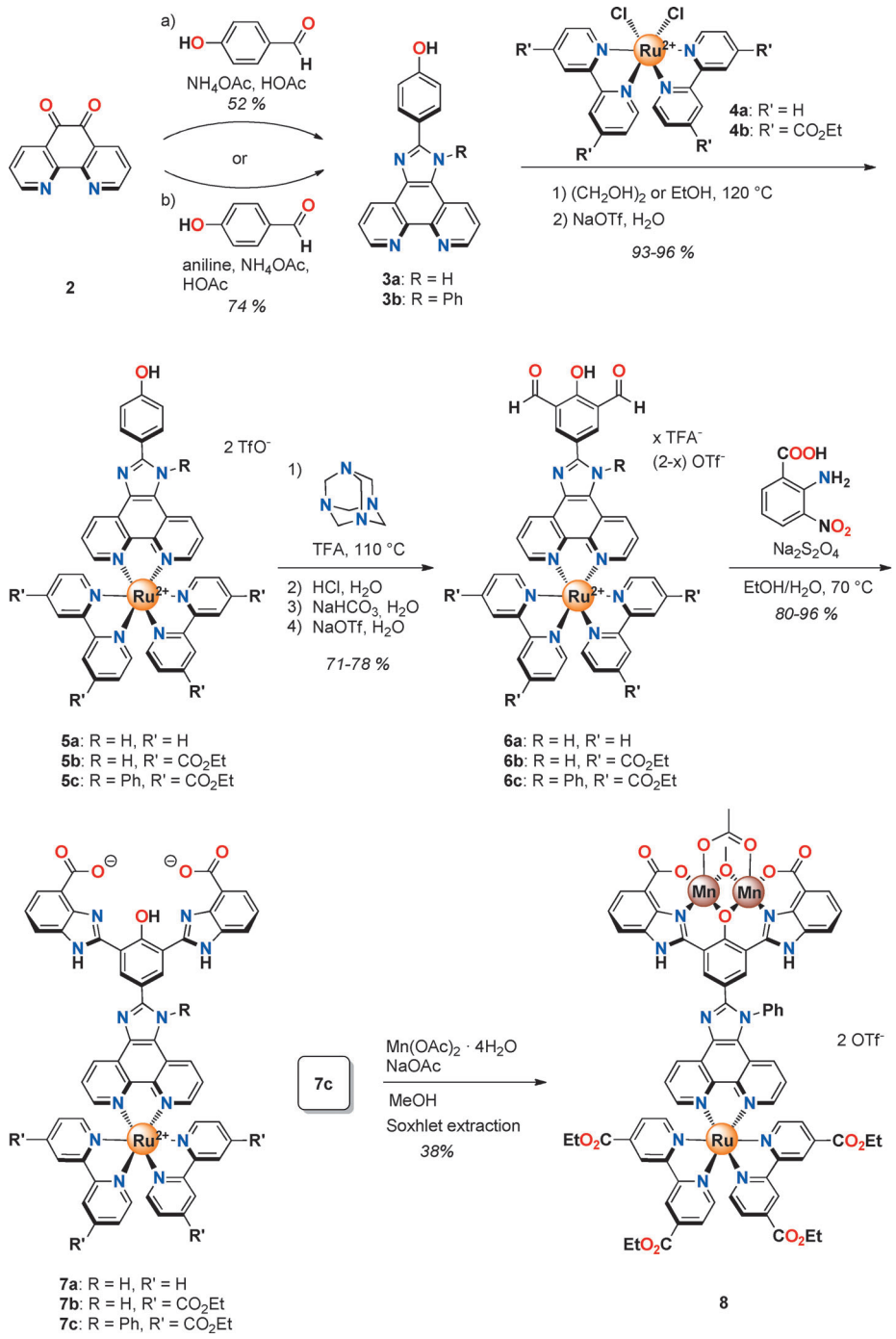

Scheme 1. Synthetic routes to **7a–c** and **8**. OTf = triflate, TFA = trifluoroacetic acid.

Adjusting the pH to 1 with HCl had a profound effect on the spectra of **7a–c** and **8**. An example is shown for **7c** in the inset in Figure 2. At neutral pH, the absorption at $\lambda \approx 450$ nm is broad, with a hump at $\lambda \approx 480$ nm, suggesting a mixed excited state that contains the MLCT state. At high pH, the spectrum is very similar, but the hump becomes slightly more visible. By contrast, at low pH, a single peak at $\lambda \approx 460$ nm appears, which is probably due to the unperturbed MLCT state, as also suggested by the long lifetime of this excited state (see below). Owing to the limited solubility of the complexes, determination of the exact molar extinction coefficients was difficult.

Table 1. Oxidation potentials for the $[Ru(bpy)_3]^{3+/2+}$-centred oxidation for complexes **7a–c** and structurally related complexes.

Compound	Solvent	*E* (V vs. NHE)	Reference
7a[a]	H_2O	1.38	this work
7b[a]	H_2O	1.60	this work
7c[a]	H_2O	1.56	this work
$[Ru(bpy)_3]^{2+}$	H_2O	1.26	[51]
$[Ru(bpy)_3]^{2+}$	acetonitrile	1.50	[51]
10	CH_2Cl_2	1.64	[48]

[a] Measured in an aqueous phosphate buffer solution (0.1 M, pH 7.2) purged with argon. Oxidation potentials were determined from DPV.

Electrochemical measurements

The limited solubility of the compounds precluded electrochemical characterisation by cyclic voltammetry and **7a–c** and **8** were therefore studied by means of differential pulse voltammetry (DPV) in phosphate buffer (0.1 M, pH 7.2), under similar conditions to those of the catalytic experiments (see below). The respective oxidative DPV results are shown in Figure 4 and summarised in Tables 1 and 2. A first redox process at 0.86, 0.87 and 0.97 V versus a normal hydrogen electrode (NHE)[49] was observed for **7a–c**, respectively; this was assigned to ligand-based oxidations, as previously reported for similar complexes.[48]

A second oxidation assigned to a metal-based oxidation of the ruthenium centre was observed at 1.38, 1.60 and 1.56 V versus NHE, respectively. The potential of the metal-centred oxidation is higher for **7a–c** than that of pristine $[Ru(bpy)_3]^{2+}$ and related complexes (Table 1), which can be explained by the presence of the electron-withdrawing imidazole-phenanthroline-type ligand. As expected, the oxidation of the ruthenium centre is shifted ($\approx$0.20 V) to higher potentials for **7b** and **7c**, which contain electron-withdrawing ester groups on the

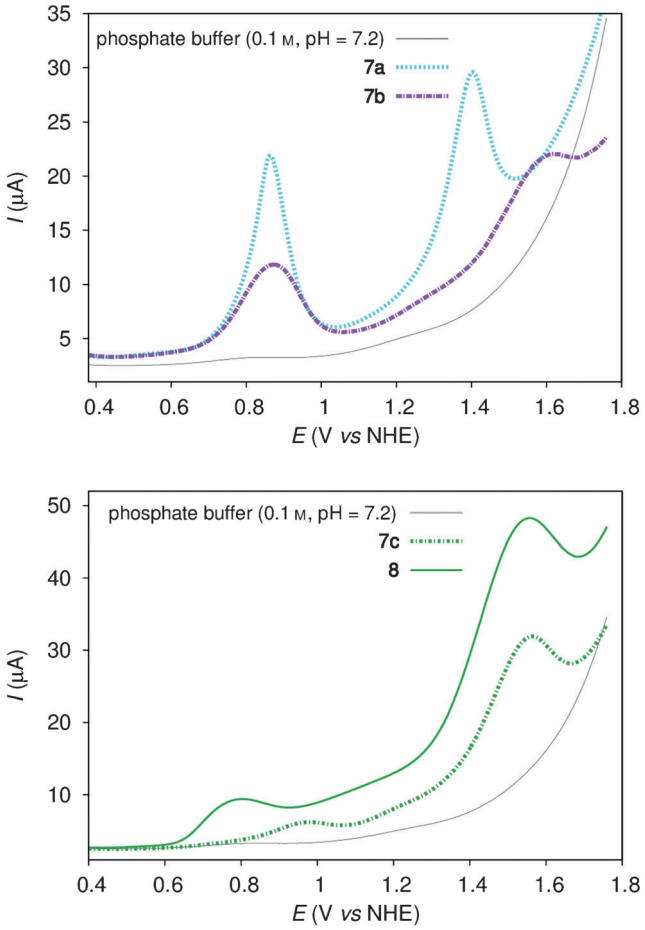

Figure 4. DPV results of **7a** and **7b** (upper), and **7c** and **8** (lower). Conditions: DPV results were recorded in aqueous phosphate buffer solutions (0.1 M, pH 7.2) containing the respective compound (0.2 mM).

bpy ligands. Such a potential difference has previously been observed by our group with $[Ru(bpy)_3]^{2+}$-type complexes **9a** and **9b**.[46,50] The metal-based oxidation potential of **7a** is rather low in comparison with related compound **10** (Table 1). However, the choice of solvents may have influenced the diverging electrochemical results.[48] The DPV results for **8** also displayed two different oxidation processes, at approximately 0.80 and 1.60 V versus NHE; the latter is attributed to a ruthenium-centred oxidation. Between the two peaks the current increased, relative to values in **7a–c**, possibly because of overlapping redox processes, owing to the introduction of manganese. Interestingly, complex **8** gave rise to a catalytic current with an onset potential at about 1.20 V versus NHE. This suggests that it is an active catalyst for water oxidation. Reductive DPV results were subsequently collected for complexes **7a–c** and dyad **8**, and are shown in Table 2.

Table 2. Electrochemical data for **7a–c** and **8**.[a]

Compound	Oxidations (V vs. NHE)	Reductions (V vs. NHE)
7a	0.86, 1.38	−0.29, −1.41
7b	0.87, 1.60	−0.41, −0.93, −1.06, −1.28, −1.42
7c	0.97, 1.56	−0.99, −1.24
8	≈0.80, ≈1.1,[b] ≈1.6	−0.50, −0.92, −1.08,−1.26

[a] Electrochemical data was obtained in aqueous phosphate buffer solutions (0.1 M, pH 7.2), purged with argon, by DPV. [b] An increase in current, but not a pure peak.

Water oxidation experiments

To study whether dyad **8** was capable of catalysing light-driven water oxidation, it was dissolved in phosphate buffer at pH 7.2 and added to sodium persulfate, which acted as the external sacrificial electron acceptor, and the solution was irradiated with visible light. However, at most, trace amounts of oxygen were detected. To ensure that the photosensitiser motif in **8** did not affect the efficiency of the manganese centre as a WOC, experiments with a chemical oxidant were performed. In a typical run, complex **8** was dissolved in phosphate buffer (pH 7.2) and $[Ru(bpy)_3]^{3+}$ was added as the chemical oxidant. Immediate oxygen evolution was observed, showing similar activity to that previously reported for WOC **1**, although the measured turnover number was only approximately one (under non-optimised conditions). Control experiments for which the $[Ru(bpy)_3]^{3+}$ oxidant was added to the aqueous phosphate buffer solution, lacking dyad **8**, resulted in negligi-

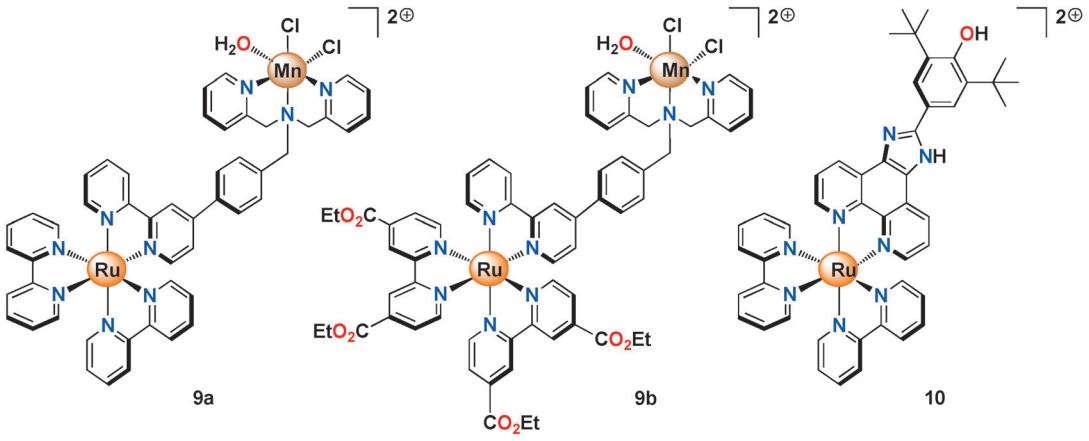

ble amounts of produced O_2. This validates that the manganese moiety in **8** is also capable of promoting oxidation of water when it is bound to the photosensitiser unit, and that the observed catalytic activity is mediated by dyad **8**.

Emission properties

Steady-state emission spectra for **5a**, **7a–c** and **8** in argon-purged mixtures of acetonitrile/water at various pH values were recorded after photoexcitation with $\lambda = 425$ nm light. To determine the effect of pH on the photophysics, the complexes were studied at different pH values and quantum yields were calculated by using $[Ru(bpy)_3]^{2+}$ as a reference. Emission maxima and quantum yields are reported in Table 3, and some examples are shown in Figure 5. All compounds exhibited a weak steady-state emission that could be attributed to ^{3}MLCT emission. Notably, compound **7a** displayed its ^{3}MLCT emission maximum at $\lambda = 613$ nm in neutral pH, whereas the maxima observed for **7b**, **7c** and **8** were $\lambda \approx 660$ nm; this clearly indicates that, if $(CO_2Et)_2$bpy ligands are present, this is where the excited state is delocalised. This is further supported by the fact that the emission maxima for **7b** and **7c** were not affected to a large extent by changes in pH, whereas for **7a** the emission maximum shifted to $\lambda = 613$ nm at neutral pH and to $\lambda = 630$ nm at low pH. Thus, in this regard the design strategy, driving the excited state further away from the manganese moiety, was successful. The quantum-yield measurements indicate unexpectedly strong quenching for the **7a–c** series, and they also revealed a strong pH dependence, such that the quantum yields were around 2–4% at low pH and decreased to <0.2% at pH 7, with a further decrease at higher pH.

Table 3. Emission properties of compounds **5a**, **7a–c** and **8** in a mixture of acetonitrile/water, at different pH values. Amplitudes (*A*) are reported as relative amplitudes and lifetimes with amplitudes lower than 4% have been omitted.[a]

Sample	A_1 [%]	τ_1 [ns]	A_2 [%]	τ_2 [ns]	A_3 [%]	τ_3 [ns]	λ_{max} [nm]	Φ [%]
5a (low)	–	–	–	–	100	858	627	–
5a (neutral)	–	–	83	92	17	584	610	–
5a (high)	–	–	30	163	70	818	621	–
7a (low)	–	–	16	339	84	1032	630	2.12
7a (neutral)	68	15	22	135	10	635	613	0.16
7a (high)	98	1.4	–	–	–	–	–	–
7b (low)	–	–	46	303	54	823	662	2.35
7b (neutral)	94	3	4	58	–	–	667	0.08
7b (high)	98	1.8	–	–	–	–	–	–
7c (low)	–	–	31	541	69	965	658	3.74
7c (neutral)	98	2.2	–	–	–	–	661	0.16
7c (high)	96	3.6	–	–	–	–	624	–
8 (low)	–	–	12	354	88	830	659	4.17
8 (neutral)	80	7.9	17.5	60.6	–	–	660	0.19
8 (high)	65	1.5	32.5	8.3	–	–	621	–
$[Ru(bpy)_3]^{2+}$[b]	–	–	–	–	100	890	611	5.90

[a] Low pH corresponds to pH 1 in aqueous solution, neutral to pH 7, and high to pH 10. The pH was adjusted by using HCl (12 M) or NaOH (5 M). [b] Data for $[Ru(bpy)_3]^{2+}$ was obtained in CH_3CN.[51]

To confirm the presence of manganese in complex **8**, photophysical control experiments were performed, in which $Mn(OAc)_2$ was added to **7c**. The ^{3}MLCT peak intensity immediately decreased. The same experiment with **8** did not result in any appreciable changes in ^{3}MLCT emission intensity; this confirmed the coordination of manganese in complex **8**. We have also recorded HRMS (ESI) spectra on solutions of complex **8**, at the concentrations used for the photophysical measurements, immediately and after standing overnight, and found no peak corresponding to free ligand **7c**. Notably, at low pH, complex **8** exhibits the highest quantum yield of all of the compounds studied. This is another indication that much of the quenching observed is due to properties of the ligand structure rather than the incorporation of manganese.

For some of the complexes (see Figure 5), the emission spectra also revealed a weak emission peak centred at $\lambda \approx 480$–500 nm. This peak had a much higher intensity at neutral and high pH relative to that at low pH, which is particularly visible for **7c**. Upon addition of $Mn(OAc)_2$ to **7c**, this peak was completely removed over the whole pH range investigated. Its nature remains elusive and is discussed in more detail (see below).

The excited-state lifetimes (see Table 3 and Figure 6) were measured in argon-purged solutions at low, neutral and high pH. From the emission decays of **5a** and **7a**, it is evident that even the excited states of precursors **5** are strongly quenched at neutral and high pH. Quenching becomes stronger when the photosensitiser is linked to the conjugated benzimidazole and phenol moieties (as in **7a**). Monitoring the emission at $\lambda = 610$ nm revealed that, at low pH, complex **5a** had one excited-state lifetime (ca. 860 ns), which corresponded to the unperturbed ^{3}MLCT state of the $[Ru(bpy)_3]^{2+}$ photosensitiser (Table 3). At neutral and high pH, complex **5a** displayed one additional shorter excited-state lifetime with significant amplitude relative to unperturbed ^{3}MLCT. At low pH, complexes **7a–c** and **8** showed similar pattern to that of **5a** at neutral and high pH, with one component with a lifetime corresponding to the unperturbed ^{3}MLCT state and one with an intermediate lifetime (300–540 ns). At high pH, complexes **7a–c** behaved very differently from that of **5a**, for which a very short lifetime, 1.4–3.6 ns, dominated. This was also true for **8**, although it also displayed a second short lifetime of 8.3 ns. Finally, at neutral pH, the excited state of complex **7a** showed triphasic decay, with one short, one intermediate and one long lifetime. In contrast, complex **7b** only displayed one major fast decay, with a lifetime of 3 ns, and a minor component with a lifetime of 58 ns. Finally, complex **7c** displayed a single fast component and complex **8** displayed a biphasic decay, similar to the pattern at high pH, with one short (ca. 8 ns) and one intermediate lifetime (ca. 60 ns).

The excited-state lifetimes corresponding to species with an emission maximum at $\lambda = 480$ nm were also determined by using the same setup. In this case, the data clearly showed that all emission components (one or two) disappeared within

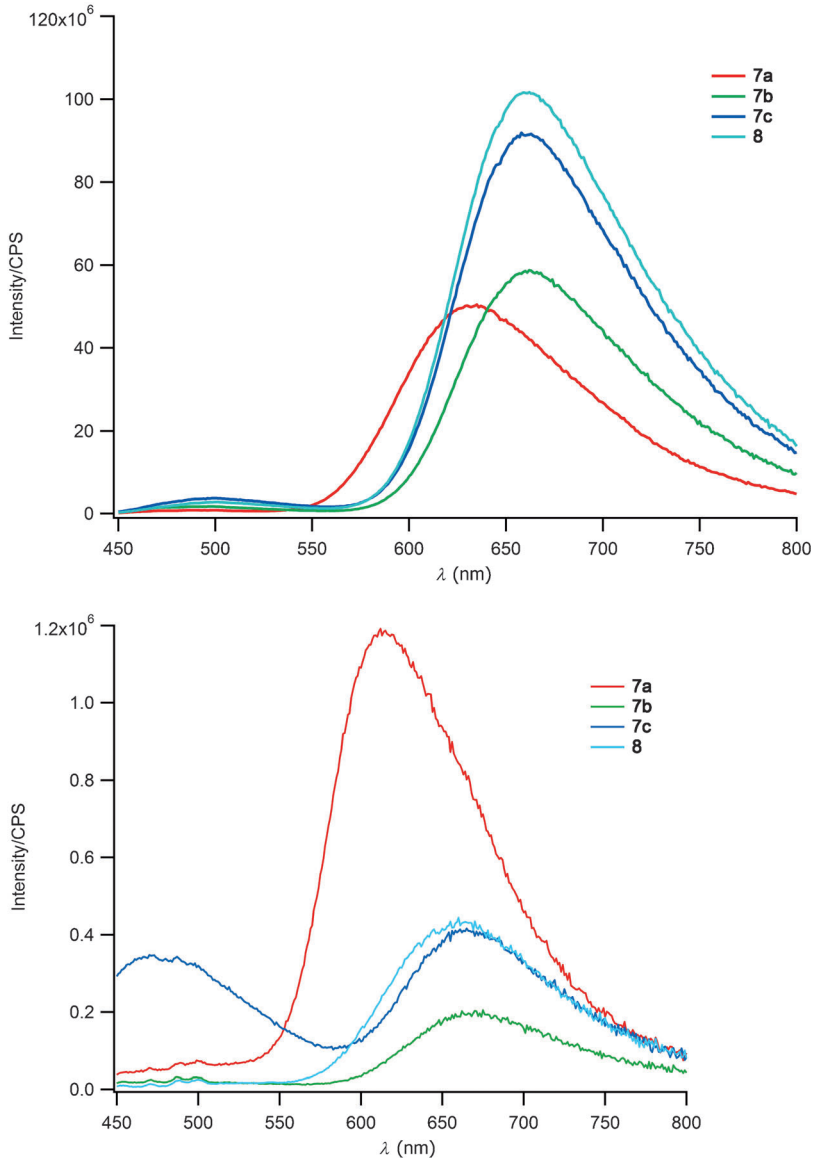

Figure 5. Emission spectra of complexes **7a**–**c** and dyad **8** in an argon-purged 1:1 mixture of acetonitrile/water (v/v) at low (upper) and neutral pH (lower). The intensities reflect the difference in quantum yield between the different dyads.

30 ns, which again highlighted that this emission did not originate from the ^{3}MLCT state.

A quantum chemical description

To shed more light on the behaviour of the complexes, TDDFT calculations were performed on **5a**, **7a** and **8**. Optimised structures for **7a** and **8** are shown in Figures 7 and 8 and Figure S3 in the Supporting Information. Complex **7a** turned out to have four different possible structures with low to moderate energies (Figure 7 and Figure S3 in the Supporting Information), whereas one structure was found for **8** (Figure 8).

The optimised structures of **7a** were found to be essentially planar (Figure 7 and Figure S3 in the Supporting Information). This is also true for **8**, for which the phenyl group at the imidazole is essentially perpendicular to the ring system and causes only a minor distortion of planarity; the dihedral angle of C1-C2-C3-N1 is 12.7° (Figure 8). It should be noted that TDDFT calculations predict the experimentally observed electronic spectra quite well; thus there is good reason to believe that the calculated geometries are relevant for our discussion. The system will thus be perfectly conjugated and manganese and ruthenium will strongly interact in **8**. This is expected to lead to the observed quenching of the excited state of the photosensitiser and prevent electron transfer from the ruthenium photosensitiser to an external acceptor. Perhaps more surprising is that the imidazole ligand itself is also a strong quencher, which will greatly interfere with this electron transfer even in the absence of manganese. The reason may be that the phenol is deprotonated or at least strongly hydrogen bonded in the relevant low-energy ground states (see below).

The lowest observed excitation for **5a** is the HOMO–LUMO transition, which is of charge-transfer character, from the phenol to π^* orbitals on bpy, and was calculated to occur at $\lambda = 451$ nm in water (Table S2 and Figure S8 in the Supporting Information), with significant oscillator strength. Geometry optimisation of the triplet state of **5a** gives the ^{3}MLCT state **5a-T$_1$**, in which the spin density is located on the bpy ligand and on ruthenium (Figure S7 in the Supporting Information). The transition from **5a-T$_1$** to S_0 corresponds to a wavelength of $\lambda =$ 641 nm from our calculations and is in close agreement with the observed value of $\lambda = 627$ nm. If **5a** is mono-deprotonated (total charge of $+1$), two isomers can be envisioned: deprotonation of the phenol (**5a$_{deprotonated}$-A**) and of the imidazole (**5a$_{deprotonated}$-B**). In the ground state, complex **5a$_{deprotonated}$-B** is more stable than that of **5a$_{deprotonated}$-A** by 7.2 kcal mol^{-1}. TDDFT calculations on **5a$_{deprotonated}$-B** show that the lowest transition is the HOMO–LUMO excitation, which corresponds to a wavelength of $\lambda = 573$ nm.

The significant redshift compared with **5a** is due to the formation of an anionic ligand. Calculations show that, in the trip-

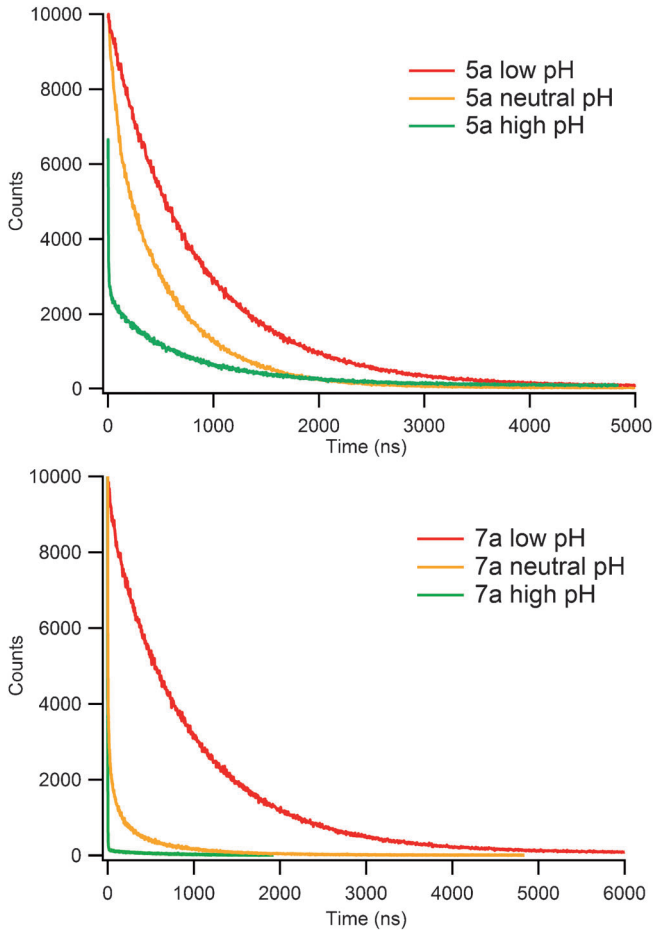

Figure 6. Time-resolved emission decay traces for **5a** (upper) and complex **7a** (lower) in a deaerated 1:1 mixture of acetonitrile/water (v/v) at different pH values for emission at $\lambda = 610$ nm.

let state, complex **5a**$_{deprotonated}$**-A** becomes 3.2 kcal mol^{-1} lower in energy than that of **5a**$_{deprotonated}$**-B**. The transition from the **5a**$_{deprotonated}$**-B** triplet to the ground-state singlet corresponds to a wavelength of $\lambda = 804$ nm, although it was predicted to occur at $\lambda = 1045$ nm for **5a**$_{deprotonated}$**-A** triplet. In contrast to the long-lived ^{3}MLCT state of protonated **5a**, both of these are π^* states that are expected to be short lived, in accordance with experimental observations. In the ground state, the proton affinity of **5a**$_{deprotonated}$**-B** is calculated to be 298.6 kcal mol^{-1}, which becomes 287.6 kcal mol^{-1} in the triplet state. This suggests that the pK_a of **5a** is decreased by approximately eight units upon excitation from the ground state to the triplet state, indicating that proton-transfer reactions should be facile.

Relative to **5a**, a redshift is observed for **7a** (to $\lambda = 494$ nm (Table S1 in the Supporting Information) from $\lambda = 451$ nm; observed $\lambda \approx 470$ nm). Because of the different hydrogen-bonding options introduced by the imidazole groups in the ligand, four possible isomers were found for **7a** in the singlet ground state. The two structures with lowest energy (**7a-S$_0$** and **7a-S$_0$-B**) are shown in Figure 7, and the other two, **7a-S$_0$-C** and **7a-S$_0$-D**, are shown in Figure S3 in the Supporting Information. In the last two isomers, the phenol proton is transferred to the connecting imidazole, which is doubly protonated. In **7a-S$_0$**, the phenol proton is intramolecularly transferred to the adjacent imidazole group to form an ion pair, whereas it is only hydrogen bonded to one imidazole unit in **7a-S$_0$-B**, which was found to be 1.0 kcal mol^{-1} higher in energy. Isodensity surface plots of selected molecular orbitals (MOs) for **7a-S$_0$** are reported in Figure S4 in the Supporting Information. The HOMO is the highly conjugated π orbital of the phenanthroline–benzimidazole ligand framework, and the LUMO is a combination of the π^* orbitals on the three ligands, with an equal distribution over the two bpy moieties and slightly higher contribution of the phenantroline motif. Because the LUMO is essentially a π^* orbital, the excited state is again expected to be short lived, as observed. In addition, HOMO-1 and HOMO-3 consist of mainly ruthenium-centred d orbitals and the HOMO–LUMO gap is calculated to be 2.86 eV (Table S1 in the Supporting Information). Isomer **7a-S$_0$** has the lowest energy and **7a-S$_0$-B** is the second lowest.

To further investigate the excited-state manifold of **7a**, several low-energy excited singlet states were found by using the TDDFT method and are reported in Table S1 in the Supporting Information. The lowest energy transition was calculated to be at $\lambda = 494$ nm in water, which corresponded to mainly HOMO–LUMO excitation and is an intraligand charge transfer (ILCT) state, as evidenced by the dipole moment change of about 10 D during excitation. Excited-state 3 in Table S1 in the Supporting Information is of MLCT character, with an absorption wavelength of $\lambda = 477$ nm. A number of transitions with great oscillator strength can be observed in the range of $\lambda = 400$–500 nm, which is in good agreement with experimental absorption spectra. From the ground-state structure, a TDDFT geometry optimisation was performed for the first singlet excited state (**7a-S$_1$**), which is assigned to HOMO–LUMO excitation and is 53.2 kcal mol^{-1} above the ground state. In **7a-S$_1$** (Figure S5 in the Supporting Information), the transition from S_0 to S_1 was calculated to occur at $\lambda = 588$ nm with an oscillator strength of 0.1486.

To obtain the theoretical emission spectra, we fully optimised the lower triplet excited states of **7a** in water. Three close-lying triplet states were obtained, which are labelled as **7a-T$_1$**, **7a-T$_2$** and **7a-T$_3$** (Figure S5 in the Supporting Information), according to their relative energies. State **7a-T$_1$** (46.5 kcal mol^{-1} higher in energy than that of **7a-S$_0$**) is an ^{3}ILCT transition and does not involve ruthenium, as confirmed by no spin density on the ruthenium metal centre (Figure S6 in the Supporting Information) and the emission from **7a-T$_1$** occurs with a wavelength of $\lambda = 679$ nm (experimentally observed at $\lambda = 620$ nm). Excited-state **7a-T$_2$** (48.7 kcal mol^{-1} higher in energy than that of **7a-S$_0$**) is a metal centred d–d transition (^{3}MC), for which the spin density at ruthenium is 1.87. In **7a-T$_2$**, the two axial Ru–N bonds are elongated to about 2.5 Å, owing to excitation of an electron to this anti-bonding orbital, which has also been observed from previous calculations on related ruthenium-based complexes.[52] The **7a-T$_3$** state (49.8 kcal mol^{-1} higher in energy than that of **7a-S$_0$**) is the result of a ^{3}MLCT, as evidenced by the spin density at ruthenium (0.97) and also at one of the two bpy ligands. Similar results have been obtained

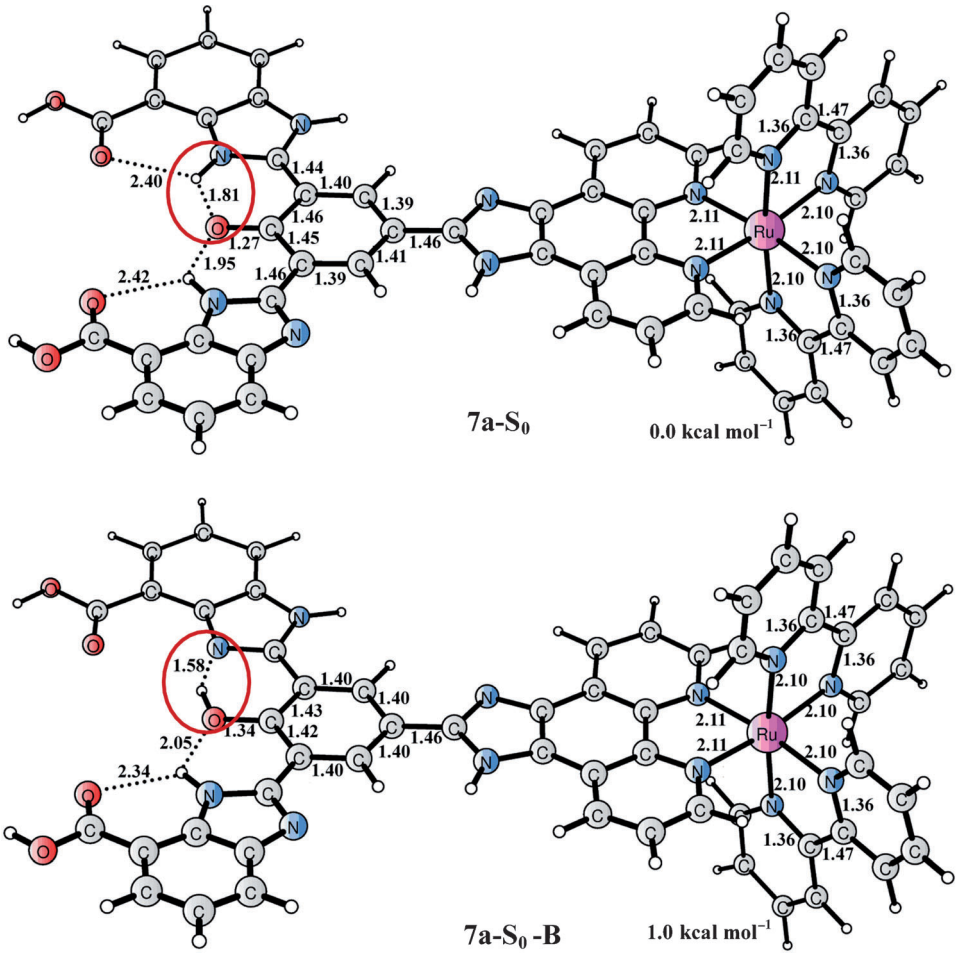

Figure 7. Two isomers of **7a** in the ground state, showing intramolecular hydrogen bonding in **7a**. Distances are given in Ångström and the relative energies are also shown.

in previous calculations on a number of ruthenium-based complexes.[52–58] The ^{3}MC states are typically extremely short lived, owing to a large non-radiative decay rate constant, and because it is close to the ^{3}MLCT state in energy, it can be expected to cause activated decay of the ^{3}MLCT state, which contributes to the short lifetime observed; this clearly also applies to **7b** and **7c**.[51] For dyad **8**, which is formally in the $Mn_2^{III,III}$ oxidation state, the high-spin ferromagnetic coupled nonet was first considered and the optimised structures are shown in Figure 8. Spin density analysis, which suggests that the electronic structure of **8** is a nonet state, can be interpreted as featuring a high-spin Mn^{II} ($S_{Mn1}=5/2$) ferromagnetically coupled to a high-spin Mn^{III} ($S_{Mn1}=2$) and antiferromagnetically coupled to a ligand radical ($S=1/2$). The ligand radical is mainly centred at the phenolate–imidazole part and at the two bpy moieties, although a small spin density can also be seen at the ruthenium centre. These results suggest that in dyad **8** the ligand backbone is oxidised rather than the second manganese. An antiferromagnetically coupled singlet state was also considered for **8** and calculations show that this state is 0.7 kcal mol^{-1} higher in energy. The singlet-state electronic structure of **8** can be described as a high-spin Mn^{II} ($S_{Mn1}=5/2$) antiferromagnetically coupled to a high-spin Mn^{III} ($S_{Mn1}=2$) and a ligand radical ($S=$

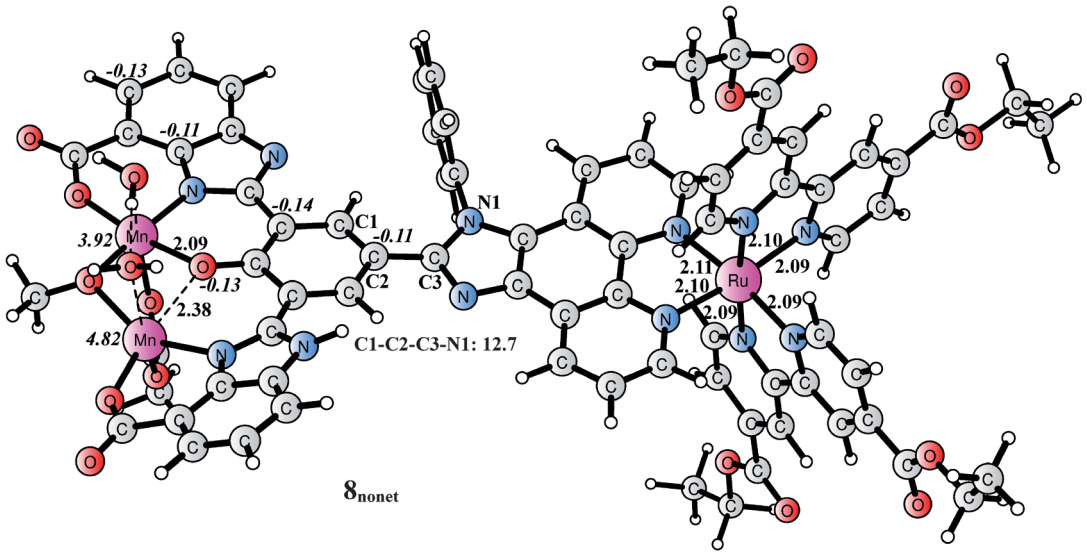

Figure 8. Calculated structure of **8**. Spin densities are indicated in italics and the dihedral angle of C1-C2-C3-N1 is indicated (in degrees).

1/2). The undectet with all three sites ferromagnetically coupled lies $+0.9\,kcal\,mol^{-1}$ higher in energy than that of the nonet.

Discussion of the quenching mechanism

We have previously shown that the quenching of the ruthenium excited state by manganese is very efficient if the manganese and ruthenium centres are in close proximity in space. As the distance between the ruthenium and manganese centres becomes shorter than about 10 Å, this results in insufficient electron transfer to the external acceptor to generate Ru^{III} owing to a diffusion-limited electron-transfer process.[39,59] Although this could be an explanation for the quenching observed for **8**, which is highly quenched compared with the parent $[Ru(bpy)_3]^{2+}$ complex, it is clear that here the quenching is also very efficient in the absence of manganese.

The finding that the excited states of the ligand complexes **7a–c** were highly quenched was initially surprising. Under neutral and basic conditions, even precursor **5a** proved to be highly quenched compared with pristine $[Ru(bpy)_3]^{2+}$. Furthermore, the fact that **5a** exhibits a bi-exponential decay under neutral conditions clearly demonstrates complex photophysical behaviour in the absence of manganese, even for this simple system. The general trend for **5a** is seen for all of the complexes studied: at low pH the emission quantum yield increases and the longer-lived components that could be attributed to more or less unperturbed ^{3}MLCT emissions are favoured. By contrast, the short-lived components became more prominent as the pH increased, and for **7** the decay became very short and essentially mono-exponential at high pH. For dyad **8**, the decay is still complex at high pH, which indeed confirms previous findings that the introduction of manganese opens up additional quenching processes that are not present in precursors **7a–c**.

When the photosensitisers were designed, it was anticipated that the phenyl ring in **7c** and **8** would have a great impact on the photophysical properties of the compounds because it could potentially destroy the planarity of the Mn_2—Ru ligand, although this does not seem to be the case. The differences between **7b** and **7c** are so small that no significant effect can be attributed to the introduced phenyl substituent. Judging from the steady-state emission data, it is clear that the ^{3}MLCT emission originates from the $(CO_2Et)_2$bpy ligands in the cases involving **7b**, **7c** and **8**, whereas it most likely resides on the phenantroline–benzimidazole part in complex **7a**. This is seen from the emission maxima, which are essentially the same for **7b**, **7c** and **8**, and is further supported by the fact that emission maxima for **7b**, **7c** and **8** are less affected by pH than **7a**; this indicates that the excited electron is delocalised over different parts of the molecule in **7a** compared with the **b** and **c** complexes. Thus, in this regard, the design strategy was successful; however, it was evidently not enough to reduce the unwanted quenching of the ^{3}MLCT state.

So, what is the origin of the quenching of **5a** and **7a–c**? NMR spectroscopy and DFT calculations suggest the presence of an intramolecular hydrogen bond between the nitrogen of the benzimidazole and the hydrogen of the phenol, resulting in a formal phenolate, which could play an important role in explaining the observed time-resolved emission of the studied dyads. As the pH is increased, more negative charge would be allocated around the phenol group and cause more efficient electron-transfer quenching from the phenolate to the excited state of ruthenium, which is essentially what is observed.

The phenol and imidazole motifs are what distinguish **5a** and **7a–c** from [Ru(bpy)]/[Ru(phen)]-type complexes, which typically give rise to mono-exponential decays with a lifetime close to 1000 ns. It is also evident that the quenching becomes stronger when the photosensitiser is linked to the combined benzimidazole and phenol moieties (as in **7**). A complex structurally related to **5a**, which has been reported by Aukauloo and co-workers, contains the phenanotroline–imidazole motif, but lacks the phenol, and yet displays a biphasic decay for which one component can be attributed to unperturbed ^{3}MLCT emission.[60]

According to the calculations, the lowest triplet state for **5a** is the expected ^{3}MLCT state, whereas for the deprotonated complex $\mathbf{5a}_{deprotonated}$ the state mainly involves the imidazole–phenantroline ligand and is ^{3}ILCT in character, which is essentially a π–π^* excited state, and is expected to be very short lived. It is possible that this state could exist in equilibrium with the ^{3}MLCT state, especially because the solvent mixture used contains both protic (water) and non-protic (acetonitrile) solvents. This type of interaction has previously been observed for assemblies with an organometallic photosensitiser attached to an aromatic backbone.[61,62]

The next question is whether this can also be used to explain the dual emission observed in the steady-state emission. Many claims of observed dual emission have turned out to be due to impurities in the sample. In this case, however, it seems more likely that both emission peaks are inherent to the samples, especially because **8** was prepared directly from **7c**, but these two complexes do not exhibit the same behaviour upon the addition of manganese to the respective samples. Thus, can the proposed equilibrium, depending on the protonation states, also explain this observed behaviour? There is indeed literature precedence for emission from derivatives of 2-(2′-hydroxyphenyl)benzimidazole that show pH-dependent emission centred at $\lambda \approx 500$ nm, just as that observed for some of the complexes in this study. The excited-state lifetimes recorded for these compounds are very similar to what we observe at $\lambda = 480$ nm: emission that decays back to the ground state in less than 30 ns.[63,64] It was suggested that the dual emission was caused by proton transfer between excited states. Because calculations show that the excited state of, for example, precursor **5a** is a strong acid, such proton transfer could also be responsible for the complex behaviour of complexes **5** and **7**. However, to ascertain that this is the reason for the observed behaviour, we would have to perform ultrafast transient absorption studies, which is beyond the scope of the current study. Irrespective of the exact mechanism, it can be concluded that the current ligand design results in quenching of the ruthenium ^{3}MLCT state that is too efficient and precludes the

desired consecutive four-electron transfer from manganese to ruthenium, and thus, also photosensitised water oxidation.

Conclusion

Three new ruthenium-containing ligands, **7a–c**, aimed at the preparation of coupled Ru–Mn_2 complexes, such as **8**, have been synthesised. Unexpectedly, these ligands turned out to have short-lived excited states, particularly at neutral and high pH. With time-resolved emission studies, it was shown that the decays of their excited states were intricate and fast, and could not be modelled with a mono-exponential decay function. The pH also proved to have a significant influence on the photophysics of the different complexes. Complementary TDDFT calculations revealed the presence of a complex excited-state manifold, as well as possible large effects of different protonation states, which may have contributed to the observed complex decay patterns. One dyad **8** was also prepared and, although it was capable of catalysing the oxidation of water, electrochemically or using $[Ru(bpy)_3]^{3+}$ as an oxidant, it failed to perform water oxidation upon illumination in the presence of an external acceptor, which was anticipated because of its short excited-state lifetime.

Although dyad **8** failed to photochemically oxidise water, the results of our study are informative and show that a highly conjugated system containing a combination of imidazole and phenol groups may affect efficient quenching of excited $[Ru(bpy)_3]^{2+}$-type photosensitisers, presumably by electron transfer from the hydrogen-bonded phenol.

Experimental Section

Materials and general methods

All reagents, including solvents, were obtained from commercial suppliers and used directly without further purification. ^{1}H NMR spectra were recorded at 400 MHz and ^{13}C NMR spectra were recorded at 100 MHz. Chemical shifts (δ) are reported in ppm relative to the residual solvent signals ([D_6]DMSO: δ(H) = 2.50 ppm and δ(C) = 39.52 ppm, D_2O: δ(H) = 4.79 ppm, CD_2Cl_2: δ(H) = 5.32 ppm and δ(C) = 53.84 ppm, $CDCl_3$: δ(H) = 7.26 ppm and δ(C) = 77.16 ppm). Splitting patterns are denoted as s (singlet), d (doublet), t (triplet), q (quartet), m (multiplet) and br (broad). High-resolution mass spectra measurements were recorded on a Bruker Daltonics microTOF spectrometer with an electrospray ioniser. The UV/Vis absorption spectra were measured on a CARY 300 Bio UV/Vis spectrophotometer. DPV measurements were performed in phosphate buffer (0.1 M, pH 7.2) with an Autolab potentiostat with a GPES electrochemical interface (EcoChemie) equipped with a glassy carbon working electrode (diameter 3 mm), a saturated calomel reference electrode (SCE) and a Pt wire as the auxiliary electrode. The redox couple $[Ru(bpy)_3]^{3+/2+}$ (E = 1.26 V vs. NHE) was used as an internal standard.

Photophysical measurements

The emission quantum yields, Φ, of **7a–c** and **8** were calculated according to Equation (1):

$$\Phi = (\eta/\eta_{ref})(A_{ref}/A)(I/I_{ref})\Phi_{ref} \quad (1)$$

in which $[Ru(bpy)_3]Cl_2$ in a 1:1 mixture of acetonitrile/water is used as a reference (which in turn is relative to the quantum yield of $[Ru(bpy)_3]Cl_2$ in acetonitrile with a value of 0.059).[51] A and A_{ref} are the absorbance values of the samples at the excitation wavelength (λ = 425 nm); I and I_{ref} are the emission intensities of the samples, given by the signed area of the emission spectra; Φ_{ref} is the quantum yield of the reference; and η is the refractive index. The excited-state lifetimes were retrieved by measuring the samples in a deaerated 1:1 mixture of acetonitrile/water (v/v) by using a λ = 405 nm pulsed picosecond diode laser as the excitation source. The detection wavelength was set at $\lambda = (610 \pm 10)$ nm. The measurement was stopped when 10000 counts had been collected in the peak channel. The emitted light was detected at magic angle and perpendicular to the excitation light through a monochromator tuned to the maximum emission wavelength of the sample. The photons were collected by a microchannel plate photomultiplier tube from Hammamatsu and fed into a multichannel analyser with 4096 channels. The excited-state decays were evaluated by using the Fluorofit software. The emission spectra of the received samples were measured on a Spex Fluorolog 3 equipped with a xenon lamp. The spectral bandwidth for the emission and excitation monochromators were 3 nm for a good signal-to-noise ratio. The spectra are a result of three averaged measurements. The excitation wavelength was λ = 425 nm for all samples. The absorbance of the samples was fixed to 0.1 ± 0.02 at the excitation wavelength. All samples were measured in a 1:1 mixture of acetonitrile/water (v/v) and the emission spectra were recorded after argon purging. To adjust the pH value, HCl (12 M) and NaOH (5 M) were used.

Water oxidation experiments

In the water oxidation experiment attempts, the gas phase of the reaction was measured by mass spectrometry. We have previously used the MS system to study oxidation of water, for further experimental details of the MS system, see refs. [18] and [65]. The light source in these experiments was a halogen lamp. Stock solutions of the dyad **8** (1 mM) were made in acetonitrile/water (1:1). The catalyst solutions used in the experiments were made by diluting the stock solutions 10 times with phosphate buffer (0.1 M, pH 7.2). The catalyst solutions (100 μM) were then deoxygenated by bubbling with N_2 for at least 5 min before use in the experiments. $Na_2S_2O_8$ (3.1 mg, 13 μmol) was placed in the reaction chamber. The system was then evacuated with a rough pump and, after the background pressure was reached, 18 mbar of He was introduced into the system. After 10 min, the catalyst (1.0 mL, 100 μM) was injected and after approximately an additional 10 min the light was switched on. The reaction chamber in these experiments was placed in a 100 mL glass with a small flow of cooling water (approximately 0.3 L min^{-1}). The function of this glass vessel was to avoid heating of the system and to act as a UV filter.

Quantum chemical calculations

DFT calculations were performed with the hybrid B3LYP[66] functional in the Gaussian 09 program.[67] Previous theoretical studies on a number of ruthenium-based systems have shown that B3LYP gives quite good results for absorption and emission spectra.[52–58] The 6-31G(d,p) basis set was used for the C, N, O and H elements, and the SDD[68,69] pseudopotential was used for Mn and Ru. All calculations were performed in water by employing the CPCM continuum model.[70] Geometry optimisations were first performed for

5a, **7a** and **8** in their ground state. For **8**, the ferromagnetically coupled high-spin state was considered. For the optical absorption spectrum of **5a** and **7a**, the ground state of which is closed shell, the 20 lowest singlet–singlet transitions were calculated by using the TDDFT method. The first excited singlet state was optimised by using TDDFT, followed by fluorescence emission spectrum calculations. Three different triplet states were optimised by using different initial guesses, and the phosphorescence emission spectrum was calculated by using TDDFT. Isodensity surface plots were constructed by using the GaussView 5 program.[71]

Synthesis

1,10-phenanthroline-5,6-dione (2): This compound was synthesised according to a previously published procedure with minor modifications.[72] A mixture of concentrated H_2SO_4 (200 mL) and concentrated HNO_3 (200 mL) were added to a mixture of 1,10-phenanthroline (20.0 g, 0.111 mol) and KBr (20.0 g, 0.168 mol) under stirring at 0 °C. The red reaction mixture was kept at reflux for 6 h and excess of $Br_{2(g)}$ was quenched by conducting the gas through a saturated aqueous solution of $Na_2S_2O_3$ by using vacuum suction at the top of the reflux condenser. After being heated to reflux, the pale orange solution was poured into 2 L of ice, resulting in a yellow/green solution. A yellow precipitate was formed by adjustment of the pH to approximately 6 with 10 M NaOH (910 mL). The suspension was divided into two parts; each part was extracted with CH_2Cl_2 (5×100 mL). The organic phases were combined, dried with $MgSO_4$ and evaporated. Recrystallisation of the orange crude product from EtOH yielded yellow needle-shaped crystals (15.6 g, 67%). ^{1}H NMR (400 MHz, CD_2Cl_2, 25 °C): δ = 9.04 (dd, J = 4.68, 1.88 Hz, 2H), 8.43 (dd, J = 7.84, 1.88 Hz, 2H), 7.56 ppm (dd, J = 7.84, 4.68 Hz, 2H); ^{13}C NMR (100 MHz, CD_2Cl_2, 25 °C): δ = 177.77, 154.35, 152.29, 135.67, 129.08, 125.22 ppm; HRMS (ESI): *m/z* calcd for $C_{13}H_{11}N_2O_3$ [**2** + MeOH + H]$^+$: 243.0764; found: 243.0767.

2-(4′-hydroxyphenyl)imidazo[4,5-*f*]-1,10-phenanthroline (3a): Compound **3a** was synthesised by using a modified published procedure.[73] A solution of **2** (10.0 g, 47.6 mmol) and NH_4OAc (73.3 g, 952 mmol) in glacial acetic acid (100 mL) was heated at 90 °C for 3.5 h. Upon removal from the heat, a solution of 4-hydroxybenzaldehyde (7.26 g, 59.8 mmol) in glacial acetic acid (100 mL) was added dropwise. After heating the mixture at 90 °C for 3 h, the mixture was poured into H_2O (2 L) and neutralised to pH ≈ 7 with an aqueous solution of NH_3 (25 wt%, 200 mL). Filtration, washing with H_2O (2 L) and acetone (2 L), and drying under vacuum resulted in **3a** as an orange compound (8.75 g, 59%). ^{1}H NMR (400 MHz, [D$_6$]DMSO, 25 °C): δ = 13.50 (s, 1H), 9.98 (s, 1H), 9.01 (dd, J = 4.28, 1.76 Hz, 2H), 8.90 (dd, J = 8.12, 1.76 Hz, 2H), 8.15–8.09 (m, 2H), 7.87–7.77 (m, 2H), 7.03–6.96 ppm (m, 2H); ^{13}C NMR (100 MHz, [D$_6$]DMSO, 25 °C): δ = 179.32, 156.55, 153.35, 137.25, 128.50, 125.84 ppm; HRMS (ESI): *m/z* calcd for $C_{19}H_{13}N_4O$ [**3a** + H]$^+$: 313.1084; found: 313.1082.

2-(4′-hydroxyphenyl)-1-phenylimidazo[4,5-*f*]-1,10-phenanthroline (3b): The condensation product **3b** was prepared according to a published procedure with minor modifications.[74] 4-Hydroxybenzaldehyde (1.162 g, 9.51 mmol) was dissolved in glacial acetic acid (22 mL) followed by addition of aniline (1.04 mL, 11.4 mmol). Compound **2** (2.00 g, 9.51 mmol) and NH_4OAc (7.34 g, 95.2 mmol) were added to this orange solution, resulting in a suspension. Another portion of glacial acetic acid (18 mL) was added and the mixture was heated at reflux for 24 h under an argon atmosphere, resulting in a colour change from dark-red to brown/yellow. After being cooled to RT, the reaction mixture was poured into water (400 mL), forming a yellow precipitate. By increasing the pH of this suspension to approximately 5 with the addition of an aqueous solution of NH_3 (25 wt%, 14 mL), more precipitate formed. The solid was collected by filtration, washed with water (300 mL) and acetone (350 mL), and dried under vacuum to yield a grey powder (2.677 g, 74%). ^{1}H NMR (400 MHz, [D$_6$]DMSO, 25 °C): δ = 9.08 (dd, J = 4.34, 1.82 Hz, 1H), 9.00 (dd, J = 8.10, 1.82 Hz, 1H), 8.93 (dd, J = 4.26 and 1.62 Hz, 1H), 7.86 (dd, J = 8.10, 4.34 Hz, 1H), 7.77–7.68 (m, 5H), 7.47 (dd, J = 8.48, 4.26 Hz, 1H), 7.43–7.38 (m, 2H), 7.33 (dd, J = 8.48, 1.62 Hz, 1H), 6.74–6.70 ppm (m, 2H); ^{13}C NMR (100 MHz, [D$_6$]DMSO, 25 °C): δ = 158.52, 152.32, 148.38, 147.29, 143.82, 143.61, 137.80, 135.07, 130.63, 130.56, 130.43, 129.72, 128.99, 127.14, 126.31, 123.73, 123.39, 122.41, 120.41, 119.44, 115.14 ppm; HRMS (ESI): *m/z* calcd for $C_{25}H_{16}N_4ONa$ [**3b** + Na]$^+$: 411.1206; found: 411.1206.

4,4′-dicarboxy-2,2′-bipyridine:[75] $K_2Cr_2O_7$ (24.0 g, 81.6 mmol) was slowly added to a solution of 4,4′-dimethyl-2,2′-bipyridine (5.0 g, 27.1 mmol) in sulfuric acid (95%, 125 mL). After addition, the reaction solution was stirred for 20 h at RT. The deep-green mixture was then diluted with cold water (800 mL), filtered and washed with water until the colour became light yellow. Subsequently, the solid was heated to reflux in nitric acid (50%, 170 mL) for 4 h and then poured over ice, diluted with water (1 L) and cooled to 5 °C. The precipitate was filtered, washed with water (5×50 mL) and acetone (2×20 mL), and finally dried under reduced pressure to yield the product as a white solid (5.0 g, 91%). ^{1}H NMR (400 MHz, 0.9 M NaOD): δ = 8.78 (dd, J = 5.2, 0.67 Hz, 2H), 8.40 (dd, J = 1.5, 0.67 Hz, 2H), 7.87 ppm (dd, J = 5.2, 1.5 Hz, 2H); ^{13}C NMR (100 MHz, 0.9 M NaOD): δ = 173.7, 156.4, 150.3, 147.0, 123.9, 121.9 ppm; HRMS (ESI): *m/z* calcd for $C_{12}H_7N_2O_4$ [*M*−H]$^-$: 243.0411; found: 243.0408.

***cis*-[Ru(bpy)$_2$Cl$_2$]H$_2$O (4a)**:[76] $RuCl_3{\cdot}xH_2O$ (assumption: x = 4, 1.6 g, 5.7 mmol), bipyridine (1.9 g, 12 mmol) and LiCl (1.7 g, 40 mmol) were heated at reflux in DMF (10 mL) for 8 h. After the reaction mixture was cooled to RT, acetone (50 mL) was added and the resultant solution was cooled at 0 °C overnight. The solid was filtered, washed with H_2O (3×15 mL) and Et_2O (3×15 mL), and dried to yield a dark-green microcrystalline product (2.0 g, 72%). ^{1}H NMR (400 MHz, [D$_6$]DMSO): δ = 9.97 (dd, J = 5.56, 1.14 Hz, 2H), 8.64 (d, J = 8.15 Hz, 2H), 8.48 (d, J = 8.15 Hz, 2H), 8.07 (dt, J = 7.76, 1.54 Hz, 2H), 7.77 (dt, J = 6.63, 1.32 Hz, 2H), 7.68 (dt, J = 7.76, 1.54 Hz, 2H), 7.51 (d, J = 5.56 Hz, 2H), 7.10 ppm (dt, J = 6.63, 1.32 Hz, 2H); ^{13}C NMR (100 MHz, [D$_6$]DMSO, 25 °C): δ = 160.18, 158.18, 153.17, 151.94, 134.54, 133.27, 125.31, 125.23, 122.82, 122.46 ppm; HRMS (ESI): *m/z* calcd for $C_{20}H_{16}Cl_2N_4NaRu$ [*M* + Na]$^+$: 506.9688; found: 506.9693.

[Ru(deeb)$_2$Cl$_2$] (deeb = 2,2′-bipyridinyl-4,4′-dicarboxylic acid diethyl ester) (4b): This ruthenium complex was synthesised according to a previously reported protocol with minor changes.[77] EtOH (99%, 7.5 mL) was added to $RuCl_3{\cdot}xH_2O$ (0.321 g, 1.23 mmol) and 2,2′-bipyridine-4,4′-dicarboxylic acid (0.60 g, 2.46 mmol) under an argon atmosphere. The reaction mixture was heated for 17 h in a sealed tube at 110 °C covered with aluminium foil. After being cooled to RT, the mixture was kept in a refrigerator for 3 h. The product was filtered and washed with EtOH, a saturated solution of $Na_2B_4O_7{\cdot}10H_2O$ in MeOH/H_2O (1:1), MeOH/H_2O (1:1) and finally EtOH to yield a black/purple powder (0.71 g, 75%). ^{1}H NMR (400 MHz, $CDCl_3$): δ = 10.45 (d, J = 5.90 Hz, 2H), 8.83 (d, J = 1.74 Hz, 2H), 8.66 (d, J = 1.74 Hz, 2H), 8.16 (dd, J = 5.90, 1.74 Hz, 2H), 7.70 (d, J = 6.00 Hz, 2H), 7.49 (dd, J = 6.00, 1.74 Hz, 2H), 4.57 (q, J = 7.14 Hz, 4H), 4.42 (q, J = 7.14 Hz, 4H), 1.52 (t, J = 7.14 Hz, 6H), 1.39 ppm (t, J = 7.14 Hz, 6H); ^{13}C NMR (400 MHz, $CDCl_3$): δ = 164.3,

163.8, 160.5, 158.2, 155.3, 152.6, 136.5, 135.2, 125.1, 124.6, 122.0, 121.7, 62.7, 62.6, 14.5, 14.3 ppm; HRMS (ESI): *m/z* calcd for $C_{32}H_{32}Cl_2N_4O_8NaRu$ $[M+Na]^+$: 795.0533; found: 795.0531.

5a: Compound **3a** (1.50 g, 4.80 mmol) and $[Ru(bpy)_2Cl_2]$ (2.07 g, 4.00 mmol) in ethylene glycol (40 mL) were heated in a round-bottomed flask at 120 °C for 20 h. The reaction mixture was cooled to RT before the addition of H_2O (720 mL), which resulted in a clear red solution. A solution of NaOTf (13.8 g, 10 mmol) in H_2O (40 mL) was added dropwise with stirring. The precipitate was collected by filtration and washed with a small amount of cold H_2O and large amounts of diethyl ether and finally dried under vacuum to give an orange powder (3.78 g, 92%). ^{1}H NMR (400 MHz, [D$_6$]DMSO, 25 °C): δ = 14.14 (brs, 1H), 10.11 (s, 1H), 9.09 (d, J = 8.22 Hz, 2H), 8.88 (d, J = 8.25 Hz, 2H), 8.84 (d, J = 7.95 Hz, 2H), 8.22 (ddd, J = 8.02, 7.94, 1.50 Hz, 2H), 8.16 (AA′ of AA′BB′, 2H), 8.11 (ddd, J = 7.91, 7.88, 1.48 Hz, 2H), 8.04 (dm, J = 5.05 Hz, 2H), 7.91 (m, 2H), 7.84 (dm, J = 5.71 Hz, 2H), 7.67–7.51 (m, 4H), 7.34 (ddd, J = 7.20, 5.68, 1.26 Hz, 2H), 7.02 ppm (AA′ of AA′BB′, 2H); ^{13}C NMR (100 MHz, [D$_6$]DMSO, 25 °C): δ = 159.64, 156.78, 156.56, 153.32, 151.44, 151.37, 149.76, 149.45, 144.99, 144.48, 137.93, 137.77, 136.87, 130.49, 130.30, 128.43, 127.87, 127.72, 127.15, 126.31, 126.05, 125.48, 124.44, 124.35, 122.27, 121.15, 120.38, 119.07, 115.96, 62.78 ppm; ^{19}F NMR (376 MHz, [D$_6$]DMSO, 25 °C): δ = −77.75 ppm; HRMS (ESI): *m/z* calcd for $C_{39}H_{27}N_8ORu$ [**5a**−2OTf−H]$^+$: 725.1346; found: 725.1362.

5b: Compounds **3a** (0.262 g, 0.84 mmol) and **4b** (0.541 g, 0.70 mmol) in EtOH (99%, 7 mL) were heated in a sealed tube at 120 °C for 19 h. The reaction mixture was cooled to RT before dilution with H_2O (126 mL) and the dropwise addition of an aqueous solution (7 mL) containing NaOTf (2.41 g, 14 mmol). The formed gel was heated at 100 °C for 1 h with slow stirring and cooled to RT with continued slow stirring, and then stored in the refrigerator overnight. The product was collected by filtration, washed with small amounts of cold water followed by a large amount of Et_2O, and finally dried in vacuum to yield an orange powder (0.88 g, 96%). ^{1}H NMR (400 MHz, [D$_6$]DMSO, 25 °C): δ = 14.13 (brs, 1H), 10.15 (s, 1H), 9.35 (d, J = 1.83 Hz, 2H), 9.33 (d, J = 1.77 Hz, 2H), 9.11 (m, 2H), 8.15 (AA′ of AA′BB′, 2H), 8.10 (d, J = 5.96 Hz, 2H), 8.08 (dm, J = 4.77 Hz, 2H), 7.91 (brm, 2H), 7.88 (dd, J = 5.83, 1.78 Hz, 2H), 7.81 (m, 2H), 7.73 (m, 2H), 7.03 (AA′ of AA′BB′, 2H), 4.46 (q, J = 7.05 Hz, 4H), 4.40 (q, J = 7.11 Hz, 4H), 1.37 (t, J = 7.12 Hz, 6H), 1.31 ppm (t, J = 7.03 Hz, 6H); ^{13}C NMR (100 MHz, [D$_6$]DMSO, 25 °C): δ = 163.47, 163.37, 159.73, 157.32, 157.06, 153.48, 153.00, 152.54, 138.40, 138.27, 138.17, 138.04, 131.04, 128.44, 126.69, 123.91, 123.84, 122.27, 120.31, 119.06, 116.00, 62.34, 62.26, 14.05, 13.98 ppm; ^{19}F NMR (376 MHz, [D$_6$]DMSO, 25 °C): δ = −77.76 ppm; HRMS (ESI): *m/z* calcd for $C_{51}H_{43}N_8O_9Ru$ [**5b**−2OTf−H]$^+$: 1013.2191; found: 1013.2189.

5c: Compounds **3b** (0.70 g, 1.80 mmol) and **4b** (1.16 g, 1.50 mmol) in EtOH (99%, 15 mL) were heated in a sealed tube at 120 °C for 19 h. After being cooled to RT, H_2O (210 mL) was added. A clear orange solution was obtained by filtration and being subsequently washed with H_2O (60 mL). The addition of NaOTf (5.16 g, 30 mmol) in H_2O (15 mL) under stirring resulted in the formation of a fine precipitate. Larger particles formed when this suspension was heated at 100 °C for 1 h. The precipitate was filtered, washed with small amounts of H_2O and large amounts of Et_2O, and dried in vacuum to give **5c** as a powder (1.94 g, 93%). ^{1}H NMR (400 MHz, [D$_6$]DMSO, 25 °C): δ = 10.04 (s, 1H), 9.36 (d, J = 1.77 Hz, 1H), 9.34 (d, J = 1.80 Hz, 1H), 9.34 (d, J = 1.78 Hz, 1H), 9.30 (d, J = 1.86 Hz, 1H), 9.24 (dd, J = 8.30, 1.31 Hz, 1H), 8.16 (dd, J = 5.29, 1.39 Hz, 1H), 8.12 (d, J = 5.83 Hz, 1H), 8.06 (d, J = 5.82 Hz, 1H), 8.01 (dd, J = 5.27, 1.23 Hz, 1H), 7.95 (dd, J = 8.19, 5.31 Hz, 1H), 7.89 (dd, J = 5.81, 1.78 Hz, 1H), 7.86 (dd, J = 5.86, 1.76 Hz, 1H), 7.83–7.66 (m, 9H), 7.61 (dd, J = 8.66, 5.25 Hz, 1H), 7.47–7.41 (m, 3H), 6.77 (AA′ of AA′BB′, 2H), 4.52–4.35 (m, 8H), 1.42–1.28 ppm (m, 12H); ^{13}C NMR (100 MHz, [D$_6$]DMSO, 25 °C): δ = 163.46, 163.44, 163.37, 163.36, 159.13, 159.11, 157.29, 157.19, 157.06, 157.04, 154.28, 153.03, 152.92, 152.54, 152.48, 150.85, 149.99, 144.57, 144.54, 138.45, 138.41, 138.33, 137.78, 136.80, 136.17, 131.42, 131.08, 130.84, 130.81, 130.61, 130.56, 128.96, 128.74, 128.57, 127.52, 126.71, 126.65, 125.87, 125.48, 123.94, 123.90, 123.82, 122.26, 121.45, 119.53, 119.06, 115.36, 115.12, 62.34, 62.30, 62.27, 14.05, 14.03 ppm; ^{19}F NMR (376 MHz, [D$_6$]DMSO, 25 °C): δ = −77.75 ppm; HRMS (ESI): *m/z* calcd for $C_{57}H_{48}N_8O_9Ru$ [**5c**−2OTf]$^{2+}$: 545.1288; found: 545.1307.

6a: Compound **5a** (1.0 g, 0.98 mmol) and hexamethylenetetramine (2.74 g, 19.5 mmol) were added to a microwave tube. The vessel was flushed with argon followed by the addition of TFA (6 mL) and finally the tube was sealed. After heating for three days at 110 °C, 4 M HCl (30 mL) was added and the mixture was transferred to a 500 mL E-flask and stirred at RT for 3 h. The pH was adjusted to approximately three with an aqueous saturated solution of $NaHCO_3$ (≈110 mL), resulting in a red and sticky fraction, which was dissolved by successively adding small portions of H_2O, vigorous stirring and decantation. The resulting slightly cloudy red solution was filtered and washed with H_2O. In total, 200 mL of H_2O was added. An orange precipitate formed upon the addition of NaOTf (3.36 g, 19.5 mmol) dissolved in water (6 mL). This suspension was left to stand overnight before final filtration and drying under vacuum. The orange product, **6a** (0.802 g, 78%; x_{TFA} = 0.904 and x_{OTf} = 1.096), appeared as a double salt with varying distribution of the triflate and trifluoroacetate anions, depending on the batch (determined by ^{19}F NMR spectroscopy). ^{1}H NMR (400 MHz, [D$_6$]DMSO, 25 °C): δ = 14.64 (brs, 1H), 10.42 (s, 2H), 9.15 (m, 2H), 8.94 (s, 2H), 8.89 (d, J = 8.22 Hz, 2H), 8.85 (d, J = 7.98 Hz, 2H), 8.22 (t, J = 7.82 Hz, 2H), 8.11 (t, J = 8.03 Hz, 2H), 8.06 (d, J = 5.20 Hz, 2H), 7.94 (m, 2H), 7.85 (d, J = 5.27 Hz, 2H), 7.67–7.53 (m, 4H), 7.35 ppm (t, J = 6.76 Hz, 2H); ^{13}C NMR (100 MHz, [D$_6$]DMSO, 25 °C): δ = 191.31, 164.13, 156.79, 156.55, 151.52, 151.38, 150.96, 149.87, 145.04, 137.96, 137.80, 133.86, 130.56, 127.88, 127.75, 124.95, 124.47, 124.39, 122.27, 120.76, 119.07 ppm; ^{19}F NMR (376 MHz, [D$_6$]DMSO, 25 °C): δ = −73.47, −77.75 ppm; HRMS (ESI): *m/z* calcd for $C_{41}H_{27}N_8O_3Ru$ [**6a**−OTf−TFA−H]$^+$: 781.1244; found: 781.1246.

6b: TFA (3 mL) was added to an argon-flushed tube containing **5b** (0.656 g, 0.5 mmol) and hexamethylenetetramine (1.402 g, 10.0 mmol). The tube was sealed and heated at 110 °C for 3 days. 4 M HCl (15 mL) was added to the reaction mixture and the red solution was quickly transferred to a 250 mL Erlenmeyer flask, and within a few minutes a dark-red sticky fraction was formed. The reaction mixture was stirred for another 3 h at RT before the pH was adjusted to approximately three with a saturated aqueous solution of $NaHCO_3$ (≈44 mL). With successive additions of small portions of water, vigorous stirring and decantation, the sticky fraction of water was dissolved. In total, 500 mL of water was used. This slightly cloudy solution was filtered before the addition of a solution of NaOTf (1.720 g, 10.0 mmol) in water (5 mL), which resulted in the formation of an orange precipitate. After keeping the suspension in the refrigerator overnight, the powder was collected by filtration, washed with a small amount of cold water and a large amount of diethyl ether, and dried under vacuum to yield **6b** (0.479 g, 71%) as a double salt, in which x_{TFA} = 0.45 and x_{OTf} = 1.55. ^{1}H NMR (400 MHz, [D$_6$]DMSO, 25 °C): δ = 14.28 (brs, 1H), 10.37 (s, 2H), 9.35 (m, 2H), 9.32 (m, 2H), 9.15 (m, 2H), 8.74 (s, 2H), 8.10 (d,

J=5.80 Hz, 2H), 8.07 (dm, J=4.81 Hz, 2H), 7.91 (br m, 2H), 7.88 (dm, J=5.40 Hz, 2H), 7.82 (m, 2H), 7.73 (m, 2H), 4.46 (q, J=7.07 Hz, 4H), 4.40 (q, J=7.01 Hz, 4H), 1.37 (t, J=7.10 Hz, 6H), 1.31 ppm (t, J=7.05 Hz, 6H); ^{13}C NMR (100 MHz, [D$_6$]DMSO, 25 °C): δ=191.24, 164.91, 163.47, 163.38, 157.33, 157.05, 153.01, 152.61, 152.02, 150.09, 138.41, 138.28, 133.48, 131.21, 126.69, 126.39, 126.13, 125.47, 123.90, 123.84, 122.26, 119.06, 62.34, 62.26, 14.05, 13.98 ppm; ^{19}F NMR (376 MHz, [D$_6$]DMSO, 25 °C): δ=−73.44, −77.76 ppm; HRMS (ESI): m/z calcd for $C_{53}H_{43}N_8O_{11}Ru$ [**6b**−OTf−TFA−H]$^+$: 1069.2089; found: 1069.2106.

6c: Compound **5c** (0.694 g, 0.500 mmol) and hexamethylenetetramine (1.402 g, 10.00 mmol) were added to a microwave tube. After purging with argon, TFA (3.0 mL) was added and the tube was sealed. The reaction mixture was heated at 110 °C for 3 days. HCl (15 mL, 4 M) was added in portions to the reaction and the mixture was quickly transferred to a 100 mL round-bottomed flask. Within a few minutes a two-phase system was formed: a red viscous mass and an almost colourless aqueous phase. After stirring at RT for 3 h, the pH was adjusted to approximately three through the addition of a saturated aqueous solution of $NaHCO_3$ (50 mL). The viscous mass was gradually dissolved by the addition of water in small portions and removal of the liquid part after each addition. The total amount of water added was 400 mL. The solution was filtered to remove undissolved particles. A precipitate was formed by the addition of an aqueous solution of NaOTf (1.721 g, 10.00 mmol) dissolved in water (3 mL) to the filtrate. The suspension was refrigerated overnight before it was filtered, washed with cold water (6 mL) and diethyl ether (200 mL), and finally dried in vacuum to yield **6c** (0.514 g, 71%; x_{TFA}=0.16 and x_{OTf}=1.84). ^{1}H NMR (400 MHz, [D$_6$]DMSO, 25 °C): δ=10.22 (s, 2H), 9.37 (m, 1H), 9.34 (m, 1H), 9.33 (m, 1H), 9.31 (m, 1H), 9.29 (dm, J=8.56 Hz, 1H), 8.17 (dm, J=5.83 Hz, 1H), 8.13 (s, 2H), 8.12 (d, J=5.75 Hz, 1H), 8.06 (d, J=5.86 Hz, 1H), 8.03 (dm, J=5.08 Hz, 1H), 7.96 (dd, J=8.30, 5.25 Hz, 1H), 7.89 (dd, J=5.80, 1.86 Hz, 1H), 7.86 (dd, J=5.81, 1.84 Hz, 1H), 7.85–7.70 (m, 9H) 7.64 (dd, J=8.63, 5.31 Hz, 1H), 7.49 (d, J=8.64 Hz, 1H), 4.52–4.35 (m, 8H), 1.43–1.27 ppm (m, 12H); ^{13}C NMR (100 MHz, [D$_6$]DMSO, 25 °C): δ=190.74, 163.46, 163.43, 163.36, 157.30, 157.19, 157.06, 157.05, 152.91, 152.55, 152.25, 151.03, 150.26, 144.74, 144.69, 138.47, 138.42, 138.36, 136.32, 136.15, 136.02, 131.47, 131.37, 131.05, 128.68, 128.54, 127.72, 127.04, 126.73, 126.67, 126.55 ppm; ^{19}F NMR (376 MHz, [D$_6$]DMSO, 25 °C): δ=−73.46, −77.74 ppm; HRMS (ESI): m/z calcd for $C_{59}H_{48}N_8O_{11}Ru$ [**6c**−OTf−TFA]$^{2+}$: 573.1238; found: 573.1252.

7a: Compound **6a** (0.682 g, 0.65 mmol) and 2-amino-3-nitrobenzoic acid (0.237 g, 1.3 mmol) were dissolved in EtOH (5.2 mL) at 70 °C. This mixture was removed from the heat and a solution of $Na_2S_2O_4$ (85 wt%, 0.799 g, 3.90 mmol) in H_2O (2.6 mL) was added. After heating at 70 °C for 5 h, the reaction mixture was cooled to RT before it was kept at 4 °C overnight. Filtration and washing with large amounts of EtOH, H_2O and acetone yielded an orange powder (0.643 g, 95%). ^{1}H NMR (400 MHz, [D$_6$]DMSO, 25 °C): δ= 14.5–13.9 (m, 3H), 9.32 (s, 2H), 9.27 (m, 2H), 8.89 (d, J=7.96 Hz, 2H), 8.85 (d, J=8.35 Hz, 2H), 8.22 (t, J=8.05 Hz, 2H), 8.11 (t, J=7.76 Hz, 2H), 8.02 (m, 2H), 7.97–7.81 (m, 4H), 7.86 (d, J=5.80 Hz, 2H), 7.76 (d, J=7.53 Hz, 2H), 7.65 (d, J=4.48 Hz, 2H), 7.59 (t, J=6.86 Hz, 2H), 7.37 (t, J=6.72 Hz, 2H), 7.29 ppm (t, J=7.78 Hz, 2H); HRMS (ESI): m/z calcd for $C_{55}H_{35}N_{12}O_5Ru$ [**7a**+H]$^+$: 1045.1891; found: 1045.1905.

7b: Compound **6b** (338 mg, 0.25 mmol) and 2-amino-3-nitrobenzoic acid (91 mg, 0.5 mmol) were dissolved in absolute EtOH (2 mL) at 70 °C in a microwave tube. A solution of $Na_2S_2O_4$ (85 wt%, 0.307 g, 1.50 mmol) in water (1 mL) was added and the tube was capped and heated at 70 °C for 5 h. After cooling to RT, the reaction mixture was stored in the refrigerator overnight. The precipitation was filtered and washed with EtOH, water and EtOH to yield a red/orange powder (320 mg, 96%) ^{1}H NMR (400 MHz, [D$_6$]DMSO, 25 °C): δ=14.4–13.9 (m, 3H), 9.40–8.95 (m, 8H), 8.18–8.01 (m, 4H), 7.98–7.80 (m, 8H), 7.80–7.60 (m, 4H), 7.30 (t, J=7.57 Hz, 2H), 4.46 (q, J=7.14 Hz, 4H), 4.39 (q, J=7.07 Hz, 4H), 1.38 (t, J=7.08 Hz, 6H), 1.31 ppm (t, J=7.10 Hz, 6H); HRMS (ESI): m/z calcd for $C_{67}H_{51}N_{12}O_{13}Ru$ [**7b**+H$^+$]$^+$: 1333.2737; found: 1333.2730.

7c: A solution of NaS_2O_4 (85 wt%, 31 mg, 0.15 mmol) in H_2O (0.1 mL) was added to a solution of **6c** (36 mg, 0.025 mmol) and 2-amino-3-nitrobenzoic acid (9.1 mg, 0.05 mmol) in EtOH (0.2 mL) dissolved at 70 °C. The reaction mixture was heated in a sealed tube at 70 °C for 5 h. A precipitate was formed upon cooling to RT. After refrigeration overnight, the suspension was filtered and washed with EtOH (8 mL), H_2O (2 mL) and EtOH (5 mL), and finally dried under vacuum to yield **7c** (28 mg, 80%). ^{1}H NMR (400 MHz, [D$_6$]DMSO, 25 °C): δ=13.96 (br s, 2H), 9.46–9.18 (m, 5H), 8.71 (br s, 2H), 8.17 (d, J=5.43 Hz, 1H), 8.13 (d, J=5.49 Hz, 1H), 8.06 (d, J=5.83 Hz, 1H), 8.00 (d, J=5.10 Hz, 1H), 7.98–7.68 (m, 16H), 7.62 (m, 1H), 7.49 (d, J=8.69 Hz, 1H), 7.28 (t, J=7.80 Hz, 2H), 4.52–4.34 (m, 8H), 1.44–1.25 ppm (m, 12H); HRMS (ESI): m/z calcd for $C_{73}H_{56}N_{12}O_{13}Ru$ [**7c**+2H]$^{2+}$: 705.1561; found: 705.1588.

Dyad 8: Complex **7c** (25.0 mg, 0.0178 mmol) was placed in a Soxhlet sock. $Mn(OAc)_2{\cdot}4H_2O$ (10.9 mg, 0.0444 mmol) and NaOAc (14.6 mg, 0.178 mmol) were added to a 25 mL flask followed by MeOH (10 mL). After Soxhlet extraction for 17 h, the resulting orange suspension was centrifuged and washed with MeOH (2× 4 mL) and dried in vacuum to yield a dark-orange powder (14 mg, 38%). HRMS (ESI): m/z calcd for $C_{75}H_{56}N_{12}O_{17}Mn_2Ru$ [**8**+2OH−MeO−2H]$^-$: 1608.1696; found 1608.1629; elemental analysis calcd (%) for $C_{78}H_{75}F_6Mn_2N_{12}O_{30}RuS_2$ (**8**+2OTf$^-$+8H$_2$O): C 45.71, H 3.69, N 8.20, Mn 5.36, Ru 4.96; found: C 45.69, H 3.47, N 9.42, Mn 5.93, Ru 5.17.

Acknowledgements

We thank the Swedish Energy Agency, the Swedish Research Council (VR), Göran Gustafsson Foundation for Natural Science and Medical Research and the Knut and Alice Wallenberg Foundation for financial support, and Professor Bo Albinsson at Chalmers University of Technology for fruitful discussions.

Keywords: electron transfer · manganese · photophysics · quantum chemistry · water splitting

[1] J. J. Concepcion, R. L. House, J. M. Papanikolas, T. J. Meyer, *Proc. Natl. Acad. Sci. USA* **2012**, *109*, 15560–15564.
[2] L. Sun, L. Hammarström, B. Åkermark, S. Styring, *Chem. Soc. Rev.* **2001**, *30*, 36–49.
[3] K. S. Joya, J. L. Vallés-Pardo, Y. F. Joya, T. Eisenmayer, B. Thomas, F. Buda, H. J. M. de Groot, *ChemPlusChem* **2013**, *78*, 35–47.
[4] H. Dau, C. Limberg, T. Reier, M. Risch, S. Roggan, P. Strasser, *ChemCatChem* **2010**, *2*, 724–761.
[5] M. D. Kärkäs, E. V. Johnston, O. Verho, B. Åkermark, *Acc. Chem. Res.* **2014**, *47*, 100–111.
[6] Y. Umena, K. Kawakami, J. Shen, N. Kamiya, *Nature* **2011**, *473*, 55–60.
[7] S. W. Gersten, G. J. Samuels, T. J. Meyer, *J. Am. Chem. Soc.* **1982**, *104*, 4029–4030.
[8] M. D. Kärkäs, T. Åkermark, E. V. Johnston, S. R. Karim, T. M. Laine, B.-L. Lee, T. Åkermark, T. Privalov, B. Åkermark, *Angew. Chem. Int. Ed.* **2012**, *51*, 11589–11593; *Angew. Chem.* **2012**, *124*, 11757–11761.

[9] C. Sens, I. Romero, M. Rodríguez, A. Llobet, T. Parella, J. Benet-Buchholz, *J. Am. Chem. Soc.* **2004**, *126*, 7798 – 7799.
[10] R. Zong, R. P. Thummel, *J. Am. Chem. Soc.* **2005**, *127*, 12802 – 12803.
[11] Y. Xu, A. Fischer, L. Duan, L. Tong, E. Gabrielsson, B. Åkermark, L. Sun, *Angew. Chem. Int. Ed.* **2010**, *49*, 8934 – 8937; *Angew. Chem.* **2010**, *122*, 9118 – 9121.
[12] M. D. Kärkäs, T. Åkermark, H. Chen, J. Sun, B. Åkermark, *Angew. Chem. Int. Ed.* **2013**, *52*, 4189 – 4193; *Angew. Chem.* **2013**, *125*, 4283 – 4287.
[13] A. Sartorel, M. Carraro, G. Scorrano, R. D. Zorzi, S. Geremia, N. D. McDaniel, S. Bernhard, M. Bonchio, *J. Am. Chem. Soc.* **2008**, *130*, 5006 – 5007.
[14] S. Maji, I. López, F. Bozoglian, J. Benet-Buchholz, A. Llobet, *Inorg. Chem.* **2013**, *52*, 3591 – 3593.
[15] M. D. Kärkäs, E. V. Johnston, E. A. Karlsson, B.-L. Lee, T. Åkermark, M. Shariatgorji, L. Ilag, Ö. Hansson, J.-E. Bäckvall, B. Åkermark, *Chem. Eur. J.* **2011**, *17*, 7953 – 7959.
[16] H.-W. Tseng, R. Zong, J. T. Muckerman, R. Thummel, *Inorg. Chem.* **2008**, *47*, 11763 – 11773.
[17] J. D. Blakemore, N. D. Schley, D. Balcells, J. F. Hull, G. W. Olack, C. D. Incarvito, O. Eisenstein, G. W. Brudvig, R. H. Crabtree, *J. Am. Chem. Soc.* **2010**, *132*, 16017 – 16029.
[18] Y. Gao, T. Åkermark, J. Liu, L. Sun, B. Åkermark, *J. Am. Chem. Soc.* **2009**, *131*, 8726 – 8727.
[19] J. Limburg, J. S. Vrettos, L. M. Liable-Sands, A. L. Rheingold, R. H. Crabtree, G. W. Brudvig, *Science* **1999**, *283*, 1524 – 1527.
[20] A. K. Poulsen, A. Rompel, C. J. McKenzie, *Angew. Chem. Int. Ed.* **2005**, *44*, 6916 – 6920; *Angew. Chem.* **2005**, *117*, 7076 – 7080.
[21] P. Kurz, *Dalton Trans.* **2009**, 6103 – 6108.
[22] W. A. A. Arafa, M. D. Kärkäs, B.-L. Lee, T. Åkermark, R.-Z. Liao, H.-M. Berends, J. Messinger, P. E. M. Siegbahn, B. Åkermark, *Phys. Chem. Chem. Phys.* **2014**, DOI: 10.1039/C3CP54800G.
[23] W. C. Ellis, N. D. McDaniel, S. Bernhard, T. J. Collins, *J. Am. Chem. Soc.* **2010**, *132*, 10990 – 10991.
[24] J. L. Fillol, Z. Codolà, I. Garcia-Bosch, L. Gómez, J. J. Pla, M. Costas, *Nat. Chem.* **2011**, *3*, 807 – 813.
[25] S. M. Barnett, K. I. Goldberg, J. M. Mayer, *Nat. Chem.* **2012**, *4*, 498 – 502.
[26] Z. Chen, T. J. Meyer, *Angew. Chem. Int. Ed.* **2013**, *52*, 700 – 703; *Angew. Chem.* **2013**, *125*, 728 – 731.
[27] M.-T. Zhang, Z. Chen, P. Kang, T. J. Meyer, *J. Am. Chem. Soc.* **2013**, *135*, 2048 – 2051.
[28] T. Nakazono, A. R. Parent, K. Sakai, *Chem. Commun.* **2013**, *49*, 6325 – 6327.
[29] M. W. Kanan, D. G. Nocera, *Science* **2008**, *321*, 1072 – 1075.
[30] A. Magnuson, Y. Frapart, M. Abrahamsson, O. Horner, B. Åkermark, L. Sun, J. Girerd, L. Hammarström, S. Styring, *J. Am. Chem. Soc.* **1999**, *121*, 89 – 96.
[31] L. Sun, L. Hammarström, T. Norrby, H. Berglund, R. Davydov, M. Andersson, A. Börje, P. Korall, C. Philouze, M. Almgren, S. Styring, B. Åkermark, *Chem. Commun.* **1997**, 607 – 608.
[32] L. Sun, M. K. Raymond, A. Magnuson, D. LeGourriérec, M. Tamm, M. Abrahamsson, P. H. Kenéz, J. Mårtensson, G. Stenhagen, L. Hammarström, S. Styring, B. Åkermark, *J. Inorg. Biochem.* **2000**, *78*, 15 – 22.
[33] P. Huang, A. Magnuson, R. Lomoth, M. Abrahamsson, M. Tamm, L. Sun, B. van Rotterdam, J. Park, L. Hammarström, B. Åkermark, *J. Inorg. Biochem.* **2002**, *91*, 159 – 172.
[34] L. Sun, H. Berglund, R. Davydov, T. Norrby, L. Hammarström, P. Korall, A. Börje, C. Philouze, K. Berg, A. Tran, M. Andersson, G. Stenhagen, J. Mårtensson, M. Almgren, S. Styring, B. Åkermark, *J. Am. Chem. Soc.* **1997**, *119*, 6996 – 7004.
[35] D. Burdinski, K. Wieghardt, S. Steenken, *J. Am. Chem. Soc.* **1999**, *121*, 10781 – 10787.
[36] D. Burdinski, E. Bothe, K. Wieghardt, *Inorg. Chem.* **2000**, *39*, 105 – 116.
[37] L. Sun, M. Burkitt, M. Tamm, M. K. Raymond, M. Abrahamsson, D. LeGourriérec, Y. Frapart, A. Magnuson, P. H. Kenéz, P. Brandt, A. Tran, L. Hammarström, S. Styring, B. Åkermark, *J. Am. Chem. Soc.* **1999**, *121*, 6834 – 6842.
[38] M. Sjödin, S. Styring, B. Åkermark, L. Sun, L. Hammarström, *J. Am. Chem. Soc.* **2000**, *122*, 3932 – 3936.
[39] K. E. Berg, A. Tran, M. K. Raymond, M. Abrahamsson, J. Wolny, S. Redon, M. Andersson, L. Sun, S. Styring, L. Hammarström, H. Toftlund, B. Åkermark, *Eur. J. Inorg. Chem.* **2001**, 1019 – 1029.
[40] S. Romain, C. Baffert, S. Dumas, J. Chauvin, J.-C. Leprêtre, D. Daveloose, A. Deronzier, M.-N. Collomb, *Dalton Trans.* **2006**, 5691 – 5702.
[41] S. Romain, J.-C. Leprêtre, J. Chauvin, A. Deronzier, M.-N. Collomb, *Inorg. Chem.* **2007**, *46*, 2735 – 2743.
[42] M.-N. Collomb, A. Deronzier, *Eur. J. Inorg. Chem.* **2009**, 2025 – 2046.
[43] C. Herrero, J. L. Hughes, A. Quaranta, N. Cox, A. W. Rutherford, W. Leibl, A. Aukauloo, *Chem. Commun.* **2010**, *46*, 7605 – 7607.
[44] C. Herrero, A. Quaranta, S. Protti, W. Leibl, A. W. Rutherford, D. R. Fallahpour, M.-F. Charlot, A. Aukauloo, *Chem. Asian J.* **2011**, *6*, 1335 – 1339.
[45] C. E. Castillo, S. Romain, M. Retegan, J.-C. Leprêtre, J. Chauvin, C. Duboc, J. Fortage, A. Deronzier, M.-N. Collomb, *Eur. J. Inorg. Chem.* **2012**, 5485 – 5499.
[46] M. L. A. Abrahamsson, H. B. Baudin, A. Tran, C. Philouze, K. E. Berg, M. K. Raymond-Johansson, L. Sun, B. Åkermark, S. Styring, L. Hammarström, *Inorg. Chem.* **2002**, *41*, 1534 – 1544.
[47] E. A. Karlsson, B.-L. Lee, T. Åkermark, E. V. Johnston, M. D. Kärkäs, J. Sun, Ö. Hansson, J.-E. Bäckvall, B. Åkermark, *Angew. Chem.* **2011**, *123*, 11919 – 11922; *Angew. Chem. Int. Ed.* **2011**, *50*, 11715 – 11718.
[48] F. Lachaud, A. Quaranta, Y. Pellegrin, P. Dorlet, M.-F. Charlot, S. Un, W. Leibl, A. Aukauloo, *Angew. Chem.* **2005**, *117*, 1560 – 1564; *Angew. Chem. Int. Ed.* **2005**, *44*, 1536 – 1540.
[49] Throughout this article, redox potentials are presented against the normal hydrogen electrode (NHE). Occasionally the referenced potentials have been determined versus different electrodes and have been converted to NHE for the purpose of comparison. For conversion constants, see: V. V. Pavlishchuk, A. W. Addison, *Inorg. Chim. Acta* **2000**, *298*, 97 – 102.
[50] E. Galoppini, W. Guo, W. Zhang, P. G. Hoertz, P. Qu, G. J. Meyer, *J. Am. Chem. Soc.* **2002**, *124*, 7801 – 7811.
[51] A. Juris, V. Balzani, F. Barigelletti, S. Campagna, P. Belser, A. von Zelewsky, *Coord. Chem. Rev.* **1988**, *84*, 85 – 277.
[52] E. Jakubikova, W. Chen, D. M. Dattelbaum, F. N. Rein, R. C. Rocha, R. L. Martin, E. R. Batista, *Inorg. Chem.* **2009**, *48*, 10720 – 10725.
[53] M.-F. Charlot, Y. Pellegrin, A. Quaranta, W. Leibl, A. Aukauloo, *Chem. Eur. J.* **2006**, *12*, 796 – 812.
[54] M.-F. Charlot, A. Aukauloo, *J. Phys. Chem. A* **2007**, *111*, 11661 – 11672.
[55] H. A. Meylemans, N. H. Damrauer, *Inorg. Chem.* **2009**, *48*, 11161 – 11175.
[56] E. Badaeva, V. V. Albert, S. Kilina, A. Koposov, M. Sykora, S. Tretiak, *Phys. Chem. Chem. Phys.* **2010**, *12*, 8902 – 8913.
[57] S. Verma, P. Kar, A. Das, H. N. Ghosh, *Dalton Trans.* **2011**, *40*, 9765 – 9773.
[58] C. I. Oprea, B. Frecuş, B. F. Minaev, M. A. Gîrţu, *Mol. Phys.* **2011**, *109*, 2511 – 2523.
[59] H. Berglund-Baudin, L. Sun, R. Davidov, M. Sundahl, S. Styring, B. Åkermark, M. Almgren, L. Hammarström, *J. Phys. Chem. A* **1998**, *102*, 2512 – 2518.
[60] A. Quaranta, F. Lachaud, C. Herrero, R. Guillot, M.-F. Charlot, W. Leibl, A. Aukauloo, *Chem. Eur. J.* **2007**, *13*, 8201 – 8211.
[61] T. A. Grusenmeyer, J. Chen, Y. Jin, J. Nguyen, J. J. Rack, R. H. Schmehl, *J. Am. Chem. Soc.* **2012**, *134*, 7497 – 7506.
[62] J. E. Yarnell, J. C. Deaton, C. E. McCusker, F. N. Castellano, *Inorg. Chem.* **2011**, *50*, 7820 – 7830.
[63] V. Khorwal, B. Sadhu, A. Dey, M. Sundararajan, A. Datta, *J. Phys. Chem. B* **2013**, *117*, 8603 – 8610.
[64] M. Novo, M. Mosquera, F. Rodriguez Prieto, *Can. J. Chem.* **1992**, *70*, 823 – 827.
[65] Y. Xu, T. Åkermark, V. Gyollai, D. Zou, L. Eriksson, L. Duan, R. Zhang, B. Åkermark, L. Sun, *Inorg. Chem.* **2009**, *48*, 2717 – 2719.
[66] A. D. Becke, *J. Chem. Phys.* **1993**, *98*, 5648 – 5652.
[67] M. J. Frisch, et al., Gaussian 09, Revision A.1, Gaussian Inc., Wallingford, CT, **2009**. See the Supporting Information for full citation.
[68] M. Dolg, U. Wedig, H. Stoll, H. Preuss, *J. Chem. Phys.* **1987**, *86*, 866 – 872.
[69] D. Andrae, U. Häußermann, M. Dolg, H. Stoll, H. Preuß, *Theor. Chim. Acta* **1990**, *77*, 123 – 141.
[70] M. Cossi, N. Rega, G. Scalmani, V. Barone, *J. Comput. Chem.* **2003**, *24*, 669 – 681.
[71] R. Dennington, T. Keith, J. Millam, GaussView, Version 5, Semichem Inc., Shawnee Mission, KS, **2009**.
[72] A. He, C. Zhong, H. Huang, Y. Zhou, Y. He, H. Zhang, *J. Lumin.* **2008**, *128*, 1291 – 1296.
[73] P. Lenaerts, A. Storms, J. Mullens, J. D'Haen, C. Görller-Walrand, K. Binnemans, K. Driesen, *Chem. Mater.* **2005**, *17*, 5194 – 5201.

[74] C. Cheng, C. Liu, F. Wu, *Bis-Phenanthroimidazolyl Compound and Electroluminescent Device Using the Same*, Patent US 2010/0253208 A1, **2010**.
[75] A. R. Oki, R. J. Morgan, *Synth. Commun.* **1995**, *25*, 4093 – 4097.
[76] B. P. Sullivan, D. J. Salmon, T. J. Meyer, *Inorg. Chem.* **1978**, *17*, 3334 – 3341.
[77] I. Katsuhiro, *Method for Producing Ruthenium Complex*, Patent JP2007031390, **2007**.

Received: February 5, 2014
Published online on March 12, 2014